


Research Article

Environmental changes in SW France during the Middle to Upper Paleolithic transition from the pollen analysis of an eastern North Atlantic deep-sea core

Tiffanie Fourcade^{1,2*} , María Fernanda Sánchez Goñi^{2,3}, Christelle Lahaye¹, Linda Rossignol² and Anne Philippe⁴

¹Archéosciences Bordeaux, UMR 6034, Université Bordeaux Montaigne, CNRS, Maison de l'Archéologie, Esplanade des Antilles, 33600 Pessac, France;

²Environnements et Paléoenvironnements Océaniques et Continentaux (EPOC), UMR CNRS 5805, Université de Bordeaux, 33600 Pessac, France; ³École Pratique des Hautes Études, EPHE PSL University, Paris, France and ⁴Laboratoire de Mathématiques Jean Leray, Nantes Université, 44322, Nantes, France

Abstract

Evaluating synchronies between climate and cultural changes is a prerequisite for addressing the possible effect of environmental changes on human populations. Searching for synchronies during the Middle-Upper Paleolithic transition (ca. 48–36 ka) is hampered by the limits of radiocarbon dating techniques and the large chronological uncertainties affecting the archaeological and paleoclimatic records, as well by their low temporal resolution. Here, we present a high-resolution, pollen-based vegetation record from the Bay of Biscay, sea surface temperature changes, additional ¹⁴C ages, and a new IRSL date on the fine-sediment fraction of Heinrich Stadial (HS) 6. The IRSL measurements give an age of ca. 54.0 ± 3.4 ka. The paleoclimatic results reveal a succession of rapid climatic changes during the Middle-Upper Paleolithic transition in SW France (i.e. D-O 12–8 and two distinct climatic phases during HS 4). Comparison of the new paleoclimatic record with chronologically well-constrained regional archaeological changes shows that no synchronies exist between cultural transitions and environmental changes. The disappearance of Neanderthals and the arrival of *Homo sapiens* in SW France encompassed a long-term forest opening, suggesting that *Homo sapiens* may have progressively replaced Neanderthals from D-O 10 to HS 4 through competition for the same ecological niches.

Keywords: Dansgaard-Oeschger cycles, Heinrich events, ¹⁴C dating, Vegetation, Bayesian age modeling, Luminescence dating, Neanderthal, *Homo sapiens*

(Received 17 May 2021; accepted 5 April 2022)

INTRODUCTION

The role of climate change as a driver of cultural changes is a recurrent topic in the current scientific literature. Some authors explain the origin of technical or demographic changes during the Mousterian, the Middle-Upper Paleolithic transition or the Neolithic through environmental changes (Richerson et al., 2005; Berger and Guilaine, 2009; Borrell et al., 2015; Defleur et al., 2020). Others postulate that expansions and contractions of eco-cultural niches have been caused by climate and environmental changes (Banks et al., 2008, 2013; Vignoles et al., 2020). Still others advocate that cultural changes are independent of environmental changes (Pétillon et al., 2016).

Of particular importance is the possible effect of environmental changes for late Neanderthal (*Homo neanderthalensis*) adaptation and its disappearance, which occurred during the Middle and Upper Paleolithic transition (ca. 50–40 ka, Greenbaum et al., 2019). Several important events took place during this period,

such as the end of different Mousterian lithic techno-complexes (LTCs); the presence of a transitional one, the so-called and still debated Châtelperronian in SW France (Higham et al., 2010; Hublin et al., 2012; Gravina et al., 2018); and the arrival of *Homo sapiens* in Western Europe, who brought the Aurignacian culture. Although debated, Châtelperronian industry is associated with Neanderthal remains and Mousterian elements (Hublin et al., 2012; Gravina et al., 2018). This LTC is characterized by Upper Paleolithic features: curved backed blades, end-scrapers, and bladelets, but also ornaments, pigments, and bone industries (e.g., d'Errico et al., 2003; Dayet et al., 2014; Ruebens et al., 2015).

The Aurignacian, and more broadly the emergence of Upper Paleolithic industries, is considered as a clear rupture with the Middle Paleolithic (Mellars, 2004) and has been subdivided in three techno-complexes—Proto-Aurignacian, Early Aurignacian, and Aurignacian—with only partial geographical overlap. The Proto-Aurignacian has been defined and located on the western Mediterranean rim within northern Italy (Bartolomei et al., 1994), the Basque country and the French Pyrenees (Laplace, 1966; Normand and Turq, 2005), SE France (Bazile, 1977; Onorati, 1986, 2006), and Catalonia (Maroto et al., 1996). It is characterized by the production of small rectilinear flakes, larger pointed, convex flakes, and large rectilinear flakes.

*Corresponding author email address: tiffanie.fourcade@u-bordeaux-montaigne.fr

Cite this article: Fourcade T, Sánchez Goñi MF, Lahaye C, Rossignol L, Philippe A (2022). Environmental changes in SW France during the Middle to Upper Paleolithic transition from the pollen analysis of an eastern North Atlantic deep-sea core. *Quaternary Research* 110, 147–164. <https://doi.org/10.1017/qua.2022.21>

Bladelets can be arranged in Dufour bladelets or Dufour subtype. Perforated shell ornaments have been found (Taborin, 1993).

Following the Proto-Aurignacian is the Early Aurignacian, whose sites containing this LTC are located from the Atlantic to the Near East. It is characterized by the presence of recurrent characters, such as carinated scrapers, blades with lateral retouches, and split-base points (Bon, 2002). The production of blades and flakes is made from distinct chains of operation depending on the activity. Blades, which are wide and thick, are produced by soft percussion on unipolar nuclei and are intended for domestic use (Tartar et al., 2005).

Determining whether these technological variabilities are associated with environmental and climatic changes, requires reliable and robust chronologies to estimate the appearance and duration of each LTC. The increasing use of chronological modeling using Bayesian statistics in archaeological sciences (Higham et al., 2010; Discamps et al., 2011; Banks et al., 2013) aims to fill this gap for SW France during MIS 5–3. Many studies on the biostratigraphy and chronology of archaeological sites in SW Europe have been carried out (Guibert et al., 2008; Vieilleveigne et al., 2008; Discamps et al., 2011; Jaubert, 2011; Jaubert et al., 2011; Discamps and Royer, 2017) to investigate the temporal variability and spatial variabilities of these LTCs during the Middle to Upper Paleolithic transition.

These technological changes occurred within the middle part of MIS 3. This time interval was marked by millennial to centennial climate changes, a succession of warming and cooling events originally detected in Greenland ice cores, the Dansgaard-Oeschger (D-O) cycles (Dansgaard et al., 1984, 1993), and in the North Atlantic (Bond and Lotti, 1995). The period between 50 ka and 36 ka includes D-O cycles 12–8 and the large iceberg discharge event called Heinrich event (HE) 4. Each cycle starts with a D-O warming event, followed by a progressive cooling, forming the Greenland Interstadial (GI) warm phase, and a subsequent cold phase called Greenland Stadial (GS) (Rasmussen et al., 2014). HE 4 was associated with the Heinrich Stadial (HS) 4 cold phase, which lasted ca. 2,000 years (Sanchez Goñi and Harrison, 2010). Deep-sea and terrestrial pollen records and speleothem archives from Europe and its margin show that D-O cycles and HEs have strongly affected European ecosystems (Fletcher et al., 2010) and, in particular, those of western France (Genty et al., 2003; Sánchez Goñi et al., 2008, 2013; Discamps et al., 2011). Marine palynology allows the reconstruction of long and continuous regional environmental sequences (Ning and Dupont, 1997; Moss and Kershaw, 2007; Oliveira et al., 2014). The comparison between pollen and other marine proxies, some of which are suitable for dating, provides good chronologies for terrestrial and marine paleoenvironmental and climate changes (Sánchez Goñi et al., 1999).

Some authors have postulated that Neanderthal disappearance was caused by a volcanic eruption (Golovanova et al., 2010) or abrupt cooling (Finlayson and Carrión, 2007). Other authors have proposed a competition between the two human groups in Western Europe (d'Errico and Sánchez Goñi, 2003; Sepulchre et al., 2007). The hypothesis of competition has been corroborated by an eco-cultural modeling approach (Banks et al., 2008) and more recently by a numerical model of interspecific competition including the “culture level” of a species as a variable that interacts with population size (Gilpin et al., 2016). Further, a new spatially resolved numerical hominin dispersal model that simulates the migration and interaction of *H. sapiens* and Neanderthals during the rapid D-O events shows that these climatic events were not

the major cause of the disappearance of Neanderthals. A realistic disappearance of Neanderthals requires the choice of *H. sapiens* as a more effective population in exploiting scarce glacial food resources as compared to Neanderthals (Timmermann, 2020).

Climate variability could have played a role in the dietary behavior of hunter-gatherer groups. Hodgkins et al. (2016) proposed that during part of the last ice age, MIS 4 and 3 (ca. 73–40 ka), treatments of carcasses (cut and percussion marks) by Neanderthals at the Pech de l'Azé IV and Roc de Marsal (Dordogne) sites were more frequent during cold than warm climates. The cold climates would be associated with nutritional stress, as Neanderthals intensified their efforts to search for calories. These studies show that changes in the strategies of subsistence, and thus in their technical adaptation, would have been conditioned by the characteristics of the ecosystems in which they lived. However, it remains difficult to disentangle the role of climatic variations and deliberate cultural choices in their subsistence strategies (Discamps et al., 2011).

The possible effect of climate change on late Neanderthal technical adaptations and their replacement by *H. sapiens* is therefore still an open question, and can only be addressed if a synchronicity is found between climatic events and biological and technological changes. SW France is one of the best regions for tackling this question due to its richness of dated archaeological sites and the availability of deep-sea pollen and speleothem-based vegetation and climatic records. However, correlating environmental and archaeological records is a complicated task due to their chronological uncertainties.

Marine archives can be dated by numerical methods such as tephrochronology, magnetic events, ^{14}C , and OSL (e.g., Kuehl et al., 1996; Stokes et al., 2003; Waelbroeck et al., 2019). However, some marine records have not been dated using these methods yet and their chronology is based on the synchronization of the $\delta^{18}\text{O}$ of planktonic foraminifera, SST, or pollen profiles with the $\delta^{18}\text{O}$ ice core record. Records younger than ca. 45 ka are most commonly based on ^{14}C dating, but regional differences in radiocarbon quantities between marine and terrestrial organisms have been demonstrated, and particularly for the reservoir effect affecting marine records (Monge Soares, 1993; Bard et al., 1994). This effect remains a major concern in the radiocarbon community, because it introduces an additional source of error that is often difficult to quantify accurately and requires a correction (Stuiver and Braziunas, 1993; Reimer and Reimer, 2001). Luminescence dating, which can avoid the problem of C reservoirs and age calibration, has been applied to many deep-sea cores in different regions (e.g., Pacific, Arctic, Baltic, and Atlantic oceans), but not in the Bay of Biscay (e.g., Wintle and Huntley, 1979, 1980; Olley et al., 2004; Armitage and Pinder, 2017).

The aim of our study is threefold: (1) document at higher temporal resolution the environmental and climatic changes in SW France during the Middle-Upper Paleolithic transition (ca. 50–40 ka) and improve its chronology; (2) create a new well-constrained chronology for the LTCs in SW Europe (i.e., Châtelperronian, Proto-Aurignacian, and Early Aurignacian); and (3) compare the paleoenvironmental changes with the new chronologically constrained succession of these LTCs. To meet these aims, we increased the sampling resolution of MD04-2845 deep-sea core (Sánchez Goñi et al., 2008) to reach a 300–400-year resolution between samples and improve the age model by adding new absolute control points using radiocarbon and IRSL dating techniques (Thomsen et al., 2008; Thiel et al.,

2011a, b; Buylaert et al., 2012; Kars et al., 2012; Lowick et al., 2012). MD04-2845 core retrieved at 45°N in the Bay of Biscay (Northeastern Atlantic) contains pollen grains and fine-grained sediments coming mainly from the hydrographic basins of south-western France and transported by rivers that have their sources in the Massif Central and Pyrenees.

PRESENT-DAY ENVIRONMENTAL SETTING

Oceanographic setting and sediment supply

The Bay of Biscay (48°N–43°N) is a gulf of the northeast Atlantic Ocean, limited geographically to the north by the northern Biscay continental margin and to the south by the Iberian-Cantabrian margin (Fig. 1). The main surface current in the Bay of Biscay is the European Slope Current (ESC), flowing northward as far as the Armorican and Celtic coasts (Pingree and Cann, 1990). In winter, the ESC reaches its maximum intensity by the intrusion of the strong Iberian Poleward Current (IPC) flowing along the Iberian margin. This current, which brings warm waters into the southeastern part of the Bay of Biscay, is known as the Navidad current and leads to the appearance of a thermohaline front along the shelf (Castaing et al., 1999). This current branches off in the Gulf and generates a cyclonic cell circulation at 46°N, 6.5°W (Colas, 2003).

Three submarine canyons are present in the Bay of Biscay: Cap-Ferret, Cap-Breton, and Torrelavega canyons. The sediment supply preserved in the marine core comes mainly from rivers in France (Jouanneau et al., 1999). Five main rivers contribute to this sediment supply: the Vilaine, Charente, Adour, Gironde, and Loire, with the latter two contributing the most (Lapierre, 1967; Jouanneau et al., 1999). The sediments of the Adour, which drains the western Pyrenees, indirectly feed the Cap-Breton Canyon (Brocheray et al., 2014; Mazières et al., 2014), although the head of the canyon became disconnected from the river in AD 1310 (Klingebiel and Legigan, 1978). The Garonne watershed feeds the Cap-Ferret canyon (Brocheray, 2015). The Gironde estuary is the most important contributor—at least 60% of its sediment reaches the Bay of Biscay (Castaing, 1981). Some of the suspended matter discharged from the Gironde estuary and the Charente is diverted northwards by river flows and density currents where it contributes to the formation of mudflats (Allen and Castaing, 1977; Castaing, 1981; Froidefond et al., 1996; Jouanneau et al., 1999). Half of the small watersheds of the Cantabrian margin are connected to small straight canyons, leading to the Cap-Breton Canyon, while others feed into a network of canyons, converging to form the Torrelavega Canyon (Brocheray, 2015). These studies show that terrestrial fine-grained (<60 µm in diameter) sediment (Weber et al., 1991) containing pollen grains in the Bay of Biscay is mainly dominated by input from the Loire and Garonne river basins.

Climate and vegetation

The climate of southwestern Europe is controlled by atmospheric perturbations from the west (e.g., Feser et al., 2015). In southeastern Bay of Biscay, winds are variable through the year, but show seasonal patterns with a northwesterly direction in spring and summer and a southwesterly position in autumn and winter (Lavin et al., 2006). The prevailing climate in the Bay of Biscay is controlled by the NAO (North Atlantic Oscillation), which is defined as the atmospheric pressure gradient between the

Azores high and the Icelandic low. Depending on its positive or negative mode, the position and intensity of the westerly winds change, bringing more or less precipitation to western Europe (Hurrell, 1995). A positive NAO leads to a higher winter storm activity over the Atlantic, warm and wet winters in northern Europe, and dry winters in southern Europe. On the contrary, a negative NAO leads to weaker winter storms crossing on a more west-to-east pathway, bringing moist air into southern Europe and cold air to northern Europe (e.g., Visbeck et al., 2001). The climate of southwestern Europe, and in particular southwestern France, from which the pollen grains come, is humid for much of the year with annual precipitation in the order of 500–1000 mm and temperatures in winter between 0–8°C and in summer between 15–22°C (Serryn, 1994).

This temperate oceanic climate allows development of the deciduous temperate Atlantic forest in western Europe (Polunin and Walter, 1985). This forest nowadays is composed of oaks (*Quercus*) in the lower elevations, associated with birches (*Betula*) on acidic soils or hornbeams (*Carpinus*) on basic soils. *Quercus* is found associated with beech (*Fagus sylvatica*) in the higher elevations, where rainfall is higher (900–1500 mm) and average annual temperatures vary between 8–10°C. In the Massif Central, the dominant conifers, *Pinus* (*Pinus sylvestris*), spruce (*Picea alba*), and fir (*Abies alba*) colonize altitudes >600 m (Ozenda, 1982). In the Pyrenees, *Fagus sylvatica* and, locally, *Abies* or *Pinus sylvestris*, occupy the montane level from 900 m above sea level, while hooked pine (*Pinus uncinata*) and rhododendrons (Ericaceae) colonize the subalpine level (Ozenda, 1982).

MATERIAL AND METHODS

Deep-sea core MD04-2845

The MD04-2845 core (45°21'N, 5°13'W, 4175 m water depth) (Fig. 1) was taken from the Dôme Gascogne, during the ALIENOR cruise, with the oceanographic vessel Marion Dufresne equipped with a Calypso piston corer (Turon et al., 2004). The marine sedimentary core is located ~350 km from the French coast and influenced by the Bottom Water (BW) flowing at >1500 m, which is composed of the cold Northeast Atlantic Deep Water (NADW) and the Antarctic Bottom Water (ABW). This core is mostly composed of hemipelagic clayey mud sediments with scattered silty strata, with carbonate contents ranging from 10–65% and an organic carbon content of <1% (Daniau et al., 2009). This core showed a well-preserved, continuous sedimentary sequence and was found not to be affected by turbidites.

Chronology

The initial chronology of core MD04-2845 covering the last 140 ka was constructed from 17 AMS ¹⁴C dates (Sánchez Goñi et al., 2008; Daniau et al., 2009) and 11 isotopic events presented in the ACER database (Sánchez Goñi et al., 2017). The new MD04-2845 core chronology is a revised version with the new addition of three radiocarbon and one IRSL dates (Table 1).

Radiocarbon dating. Three AMS ¹⁴C dates were obtained at Beta Analytic Inc (USA) on samples of monospecific planktonic foraminifera—*Neogloboquadrina pachyderma* (s)—from the levels of maximum abundance of this species, at depths 1164, 1191, and 1226 cm, corresponding to HS 4. Dating required ~10 g of foraminifera. The reservoir effect in the Bay of Biscay was calculated from 10 stations, located from Brittany to the Arcachon basin

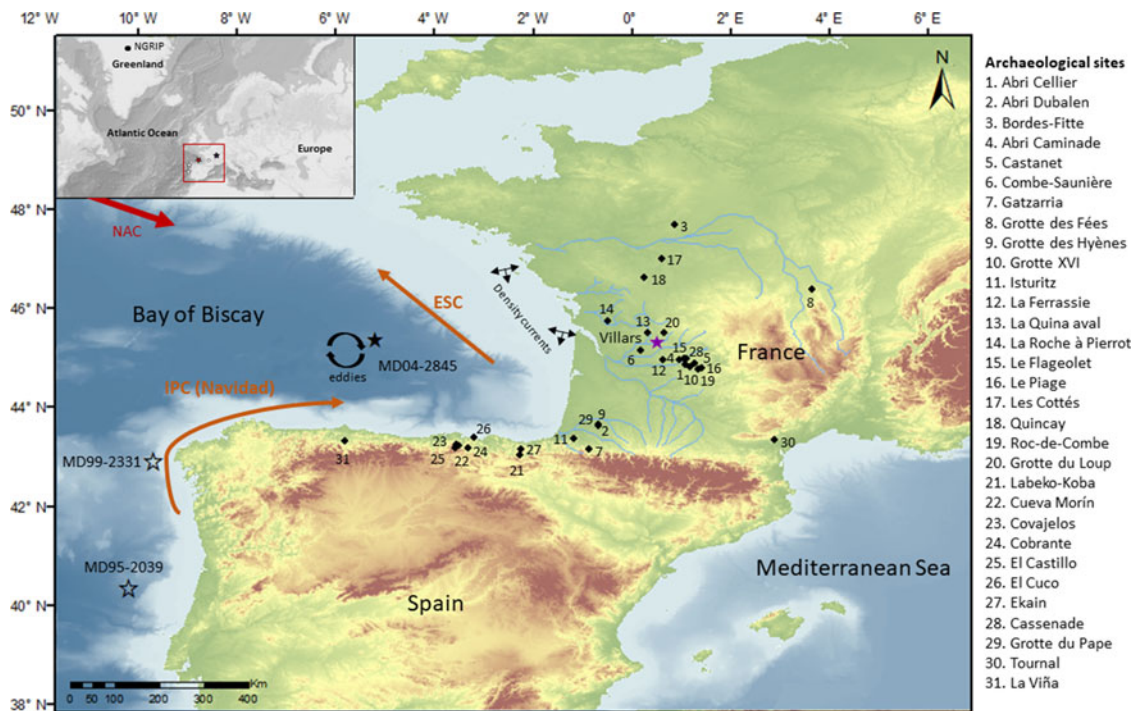


Figure 1. Partial European map showing the location of the MD04-2845 deep-sea core (black star) and the other cores discussed in the text: Iberian deep-sea cores (white stars) MD99-2331 (Naughton et al., 2009) and MD95-2039 (Roucoux et al., 2005), Greenland ice core (NGRIP, black square) (Rasmussen et al., 2014), and Villars Cave speleothem (purple star) (Genty et al., 2010). Major western rivers (blue lines) and Middle-Upper Paleolithic transition archaeological sites available in the database (black diamonds) are located on the map. The main oceanic currents and their names are represented in orange and red arrows (modified from Mary et al., 2017).

Table 1. ^{14}C , IRSL, and biostratigraphic ages with their respective uncertainties and depths used in the Bayesian depth-age model. The calendar ages of D-O events (D-O 10–17) are based on the tuning between increase in Atlantic forest from MD04-2845 deep-sea core and rapid warming events at the start of GIs, that have an estimated age and *uncertainties (Wolff et al., 2010; Rasmussen et al., 2014).

Laboratory ID/event	Depth (cm)	^{14}C age (ka BP)	Error (\pm ka BP)	Calendar age (ka)	Error* (\pm ka)	References
SacA-002977	1048	29.87	0.39			Sánchez Goñi et al., 2008
SacA-002978	1060	30.67	0.42			Sánchez Goñi et al., 2008
SacA-002976	1078	31.35	0.46			Sánchez Goñi et al., 2008
Beta-491854	1164	33.92	0.22			This study
Beta-491855	1191	33.39	0.20			This study
Beta-491856	1226	34.14	0.24			This study
D-O 10	1260			41.41	0.82	Sánchez Goñi et al., 2008
D-O 11	1290			43.29	0.87	Sánchez Goñi et al., 2008
D-O 12	1335			46.81	0.96	Sánchez Goñi et al., 2008
D-O 14	1450			54.17	1.15	Sánchez Goñi et al., 2008
D-O 17	1510			59.39	1.29	Sánchez Goñi et al., 2008
BDX24931	1535–1545			53.60	3.4	This study

(Broecker and Olson, 1961; Mangerud et al., 2006; Tisnéat-Laborde et al., 2010), and recorded online in the Marine Reservoir Database (Reimer and Reimer, 2001). The calculated reservoir age is 383 ± 53 years.

Luminescence dating. The analytical strategy for dating the MD04-2845 core was to select layers containing ice rafted detritus

(IRD)—coarse sediments coming from the melting of massive ice-berg discharges in the North Atlantic from the fragmentation of the Laurentide (HS) or from the European ice sheets. We assumed as a working hypothesis that either the IRD was exposed to the sun just before covering by the ice cap, or that the luminescence signal had been reset by the shearing of ice sheets (Bateman et al., 2012, 2018). The ice breakup allowed for iceberg discharges,

estimated to last from 50–1,500 years (Roche et al., 2004; Ziemen et al., 2019), that produced additional sediment supply and larger grain sizes, thus optimizing the quantity and quality of the sampled material. The MD04-2845 core was stored at the EPOC laboratory (Université de Bordeaux) in a refrigerated and dark environment, ideal conditions for luminescence dating. Due to the inherent constraints of the method (exposure to light), we worked on the archive part, whose surface was only exposed to light during core cutting. We sampled three levels at 936–944 cm, 1076–1081 cm, and 1535–1545 cm depths, containing IRD and the first and third ones corresponding to HS 3 and HS 6, respectively, and the second one to a very low-IRD layer (Supplementary Fig. 1). The samples were collected according to protocols described by Armitage and Pinder (2017) and Nelson et al. (2019). The samples were sieved, but only the sample corresponding to depths of 1535–1545 cm provided enough grains for dating. Due to the small amount of available material, the 41–60 μm grain size fraction was selected because it was the most abundant in proportion. The grains were successively treated with HCl (10%) and then H_2O_2 (30%) for 24 hours to remove carbonates and organic matter, respectively. They were then treated with 10% HF for 10 minutes to clean the grain surfaces and finally treated with 10% HCl to remove all fluorides eventually created during the precedent step. After rinsing and drying, the polymineral fraction was mounted on stainless steel cups previously sprayed with silicone oil using a 1 mm mask. The pIR-IR₂₉₀ luminescence signals were measured at the Archeosciences Bordeaux laboratory (Univ. Bordeaux Montaigne) using a Freiberg Instruments Lexsyg SMART reader with an internal beta $^{90}\text{Sr}/^{90}\text{Y}$ source delivering a dose rate of 0.171 ± 0.004 Gy/s (Risø calibration quartz batch 113, Hansen et al., 2015) to the polymineral fraction at the time of measurement. The fraction was stimulated with near-infrared diodes emitting at 850 nm. The IRSL signal was detected in the blue-violet region with an H7360-02 Photon Counting Head in the UV/Vis region (410 nm) through a combination of optical filters (Schott BG3, 3 mm + Semrock 414/46 BrightLine HC interference filter) placed in front of a Hamamatsu H7360-02 photomultiplier tube (PMT). The equivalent dose (D_e) was determined using the IRSL single-aliquot regenerative dose (SAR) protocol (Murray and Wintle, 2003) adapted for the pIR-IR₂₉₀ protocol (Supplementary Table 1), with a stimulation temperature of 50°C followed by a high temperature measurement at 290°C (pIR-IR₂₉₀) (Thiel et al., 2011a). The data analysis was performed with Analyst software (Duller, 2015). For each aliquot ($n = 20$), pIR-IR₂₉₀ measurements passed all acceptance criteria: the recycling ratio averages 1.01 ± 0.03 , within 5%, the recuperation ratios were also $<5\%$, and the maximum paleodose error is $<10\%$. pIR-IR₂₉₀ curves are provided for the sample (Fig. 2). D_e value was calculated using the CAM (Central Age Model) (Galbraith et al., 1999), an arithmetic average and the Average Dose Model (Guérin et al., 2017). The D_e results are similar in all three cases (Table 2) and equal within uncertainties.

The external alpha, beta, and gamma dose rates received by feldspar grains were deduced from high-purity low-background BEGe gamma spectrometry measurements (Guibert and Schwoerer, 1991). No significant disequilibrium in U-series was detected (Table 3). The internal dose rate of the feldspars was derived from internal K contents, assumed to be $12.5 \pm 0.5\%$ (Huntley and Baril, 1997). An a -value of 0.08 ± 0.02 was assumed (Rees-Jones, 1995). The most important issue is the water content, which could lead to a significant underestimation or overestimation of the age obtained (Aitken, 1998). There exists a large

variability in water content values considered for marine sediments in the previous studies (Supplementary Table 2). A value of 40% water content was measured and confirmed by further measurements (33–43%) of other samples in the core. An uncertainty value of 10% was assigned to cover all realistic uncertainties. Considering the depth of the sample, we also estimated that the cosmic dose received was negligible (Prescott and Hutton, 1994; Supplementary Table 2).

Bayesian age-depth model. A new depth-age curve was developed using all available radiocarbon ages, the paleodosimetric age obtained in the present study, and five isotopic events (Table 1). The model, named BaCON (Blaauw and Christen, 2011), is a Bayesian age modeling in sedimentary sequences that requires mainly prior information about sedimentation rates, which is difficult to obtain for long sedimentary sequences. This type of model (i.e., BaCON) does not handle sudden variations in sedimentation rates, which are found during periods of deglaciation and ice rafted debris deposition (Sánchez Goñi et al., 2017). On the contrary, our Bayesian modeling used in Archaeological Sciences does not consider sedimentation rate as a prior for Bayesian analysis embedded in the chronological model (Lanos and Philippe, 2018). For this reason, we used the ChronoModel v. 2.0 software (Lanos and Dufresne, 2019) to construct the most reliable chronological model for core MD04-2845. The prior information included in the model is a stratigraphic order according to the depth of dated samples (see Lanos and Philippe, 2018, for a description of the chronological model). The calibration step for radiocarbon ages was performed using Marine20 (Heaton et al., 2020). The posterior distribution of collection dates/ages is approximated using samples simulated by Markov chain Monte Carlo (MCMC) algorithms. Then, the MCMC samples from the joint posterior distribution are analyzed in the ArchaeoPhases R-package v. 1.4.5 (Philippe and Vibet, 2020).

Firstly, we represent the 95% credible interval for each dated sample of our collection (Fig. 3). The credible interval is calculated from the posterior distribution of each dated sample. This is the shortest interval that contains the date of sample with 95% posterior probability (i.e., there is a 95% probability that the unknown date of sample falls within this interval). Then, we estimate the age-depth curve from this sequence of ages and their depth. The curve is estimated using the classical local regression (LOESS), which is applied to express the age as a function of depth. The estimate of the curve depends on the collection of ages, which are unknown, but their posterior distribution is provided by the chronological model. Thanks to the MCMC sample, we can easily estimate the posterior distribution of the depth-age curve at each value of the depth. Therefore, we can predict the age of undated levels. For each depth value, we summarize the posterior distribution of age by its median value and 68% and 95% credible intervals.

Pollen study

Fifty-five new samples were analyzed between 1134–1317 cm depth, corresponding to a resolution of 300–400 years. The extraction protocol consists of sieving about 2–5 cc of sediment at 150 μm to separate the lower fraction containing pollen and the upper fraction composed mainly of foraminifera. A known concentration of an exotic spore, *Lycopodium*, was added to the sediment at the beginning of the treatment to calculate the total spore-pollen concentration and that of each taxon (Stockmarr, 1971). This sediment was chemically attacked (cold HCl at 10%, 25%, and 75%, and cold HF at 45% and 75%) to remove

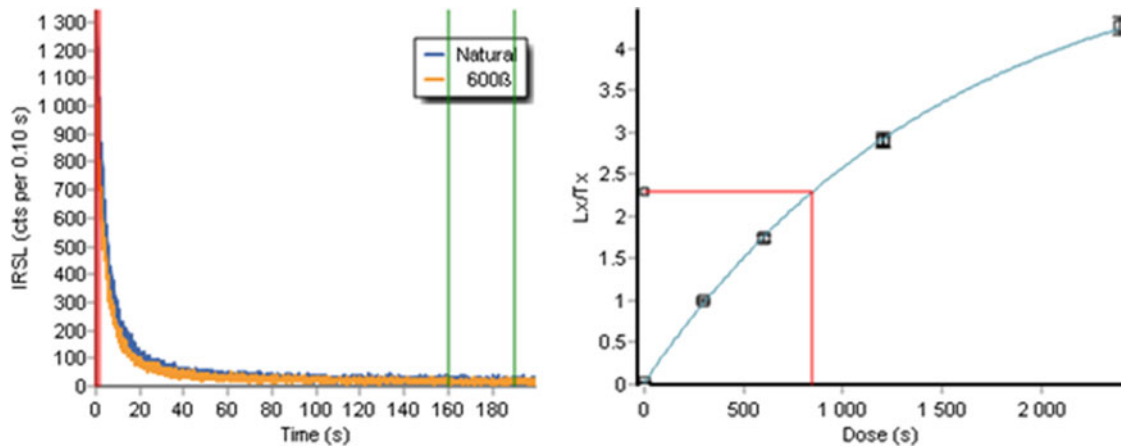


Figure 2. Decay curves and dose-response of the sample BDX24931 using pIR-IR₂₉₀ signal. On the left side of the figure, the green lines delimit the background noise, which is subtracted from the signal. The red lines on the right side of the figure are the graphical representation of how an equivalent dose (D_e) is calculated.

Table 2. Equivalent doses (D_e) obtained with the Average Dose Model (ADM) and Central Age Model (CAM), from pIRIR₂₉₀ measurements. The overdispersion (OD) values were determined with the Central Age Model. The age integrated in the age-depth model was determined with the Central Model Age.

Sample	D_e (Gy) CAM	D_e (Gy) ADM	D_e (Gy) Arithmetic average	OD (%) CAM	Age (ka) CAM	Age (ka) ADM
BDX24931 (GdG18 OSL 1)	156 ± 3	156 ± 4	156 ± 13	8 ± 2	53.6 ± 3.4	53.6 ± 4.0

carbonates and silica. The pollen residue was then filtered through a nylon filter of 10 μm and mounted on a microscope slide in a bi-distilled glycerin medium, which allows the mobility of pollen grains and their identification in polar and equatorial view. For each sample, at least 20 taxa and a main sum of >100 pollen, excluding *Pinus*, were counted using a Zeiss Axioscope optical microscope at magnifications $\times 400$ and $\times 1000$ (immersion oil). *Pinus* is over-represented in marine sediments (Heusser and Balsam, 1977) and including it in the pollen main sum would mask variations in the percentages of other pollen taxa. The sum of pollen grains excluding *Pinus* ranges from 59–151 (including pine, from 184–888 grains), with only six samples having pollen sums between 59–100 pollen grains. Pollen percentages were calculated on the total pollen counted, excluding *Pinus*, aquatic plants, spores, and undetermined pollen grains.

The different pollen taxa were grouped by their ecological affinity into five main ecological groups (Fig. 4): (1) Atlantic deciduous forest, composed mainly of deciduous *Quercus*-type, *Alnus*, *Corylus*, *Carpinus*, and *Fagus*; (2) boreal forest, formed by *Abies* and *Picea*; (3) semi-desert plants formed by *Amaranthaceae*, *Ephedra distachya*, and *E. fragilis* types; (4) heaths and heathers of the family *Ericaceae*, including the species *Calluna*; and (5) Central European steppe, composed mainly of *Artemisia*, *Cyperaceae*, and *Poaceae*.

Zonation of the pollen diagram has been carried out by clusters or hierarchical groupings, constrained by a matrix of Euclidean distance between each sample (CONISS) (Grimm, 1987). This analysis was performed in the RStudio v. 1.2.5019 environment using the *chclust* program in the *Rioja* 0.9-21 package (Juggins, 2019). The number of significant pollen zones was determined using optimal partitioning with minimal sum-of-squares and broken-stick method using *vegan* v. 2.5-7 R-package (Oksanen et al., 2020).

Principal Components Analysis (PCA) was applied to the pollen percentages to reduce the dimensionality for detecting

climatic and environmental fluctuations. Of the 125 western European taxa (excluding *Pinus*, spores, and unidentified pollen grains), 72 taxa were retained to create the PCA without standardization. However, a matrix reduction was applied to select only major taxa with pollen percentages >6% in at least 5 samples (Fig. 5). Prior to the analysis, a Hellinger transformation was used (Legendre and Gallagher, 2001) to normalize the variance of the different taxa and make it therefore more suitable for Euclidean-based ordination methods, such as PCA. The Hellinger transformation was made using the *R-vegan* package (Oksanen et al., 2020). Then, the values according to the dimension scores were extracted for each sample. Another PCA taking into account the pollen zones, was made to determine the environmental significance of these pollen zones. The analysis was carried out in the RStudio environment with three packages—*factoMineR* v. 2.3 (Husson et al., 2017), *factoextra* v. 1.0.7 (Kassambara and Mundt, 2020), and *paleoMAS* v. 2.0.1 (Correa-Metrio et al., 2012)—to extract and visualize the results of the multivariate data.

Analysis of foraminifera assemblages and SST quantitative reconstruction

Foraminifera assemblages of the MD04-2845 deep-sea core have been published previously (Sánchez Goñi et al., 2008). Here, we present data for the three new samples (levels 1164, 1191, and 1226 cm), which were dated by ^{14}C . The assemblages were analyzed in the >150 μm fraction of the same sample used for pollen analysis. Between 362–382 foraminifera were counted in these three samples. Quantitative values of seasonal and annual sea surface temperatures (SST) from planktonic foraminifera assemblages were reconstructed. This reconstruction used a paleoecological reconstruction program developed at the EPOC laboratory, based on modern analogues previously applied to this core (Sánchez Goñi et al., 2013). This reconstruction relies on an extended modern database using North Atlantic and Mediterranean samples (1007 points).

Table 3. Summary of water content, calculated equivalent dose, dose rates, paleodose, and age obtained. K, U, and Th contents were determined by high-resolution and low-background BEGe gamma spectrometry.

Sample	Depth (cm)	Water content (%)	D _e (Gy) CAM	Equivalent dose							
				K (%)	U (²³⁸ U) (ppm)	U (²³⁶ Ra) (ppm)	Th (ppm)	alpha	Beta (ext + int)	gamma	total
BDX24931	1535–1545	40 ± 10	156 ± 3	2.37 ± 0.04	2.96 ± 0.04	2.71 ± 0.15	10.35 ± 0.12	0.19 ± 0.03	1.81 ± 0.04	0.95 ± 0.08	2.91 ± 0.05

Middle and Early Upper Paleolithic lithic techno-complexes

We have created a database initially containing 32 sites and ~300 previously published ages. To this database, we applied a series of qualitative methodological, taphonomic, and sampling criteria, from 0–3 following Guibert et al. (2008), to select the most relevant ages (Excel file in Supplementary Information). The ages with index 3 are the most reliable and were integrated in the Bayesian models to reconstruct the temporal range of each LTC in each archaeological site. A model for each site was carried out with ChronoModel v. 2.0.18 (Lanos and Dufresne, 2019), taking into account the archaeostratigraphy between the different dated levels and using the most recent IntCal20 calibration curve (Reimer et al., 2020). As for the age model of core MD04-2845, ChronoModel has the advantage of integrating multiple dated ages for the same event/sample and it is able to deal statistically with the outliers. Then the events were organized in phases (i.e., archaeological levels associated with a LTCs), only constrained stratigraphically within each site. We have chosen not to impose a chronological succession of these three LTCs, because although they could be stratified in the same site, they are not necessarily all contemporaneous from Aquitaine to northern Spain. Ages of archaeological levels below and above the targeted levels (i.e., Châtelperronian, Proto-Aurignacian, and Early Aurignacian) served as boundaries. However, the Early Aurignacian corpus needs further improvement, because only the ages corresponding to the Early Aurignacian levels of the sites delivering first Proto-Aurignacian and/or Châtelperronian layers have been integrated. The prior information included in the model is a stratigraphic order according to archaeological sequence. The posterior distributions and the HPD regions at 68.2% and 95.5% were approximated for each collection events and phases (Supplementary Information). We performed the age modeling for thirteen sites. However, among them, two sites provided only one age to include in the presentation and discussion of the results (Supplementary File 2).

RESULTS

Dating the Bay of Biscay core: results and improvements

The new ¹⁴C dates range from 33.9 ± 0.2 to 34.1 ± 0.2 ¹⁴C yr BP (Table 4). The time interval corresponding to HS 4 in several North Atlantic cores (Elliot et al., 1998, 2001, 2002) is estimated between 33.9 ± 0.7 and 34.9 ± 1.1 ¹⁴C yr BP, while farther south on the Iberian margin it is dated between 33.7–34.7 ¹⁴C yr BP (Naughton et al., 2009) (Supplementary Figure 2, Supplementary Table 3). Chronological uncertainties for our AMS ¹⁴C dates range from 390–460 years (2σ error), and those based on the marine isotopic events have uncertainties between 817–1287 years (Wolff et al., 2010; Sánchez Goñi et al., 2017). The new ¹⁴C ages appear to be statistically indistinguishable in terms of uncertainties (Table 4, Supplementary Fig. 2). These ages do not yield a consistent series of increasing age with increasing depth, perhaps due to variations in the marine age reservoir. Marine reservoir age simulations have highlighted variations in global mean marine reservoir ages of several hundreds of years, especially between ca. 42–38 ka close to the Laschamp (ca. 42.9–41.5 ka, Lascu et al., 2016) geomagnetic excursion (Butzin et al., 2020; Heaton et al., 2020).

The pIR-IR₂₉₀ age obtained is 53.6 ± 3.4 ka (Table 2). This age, if considered with its uncertainty at 1 sigma, is younger than the other ages from other records for the HS 6, which is estimated

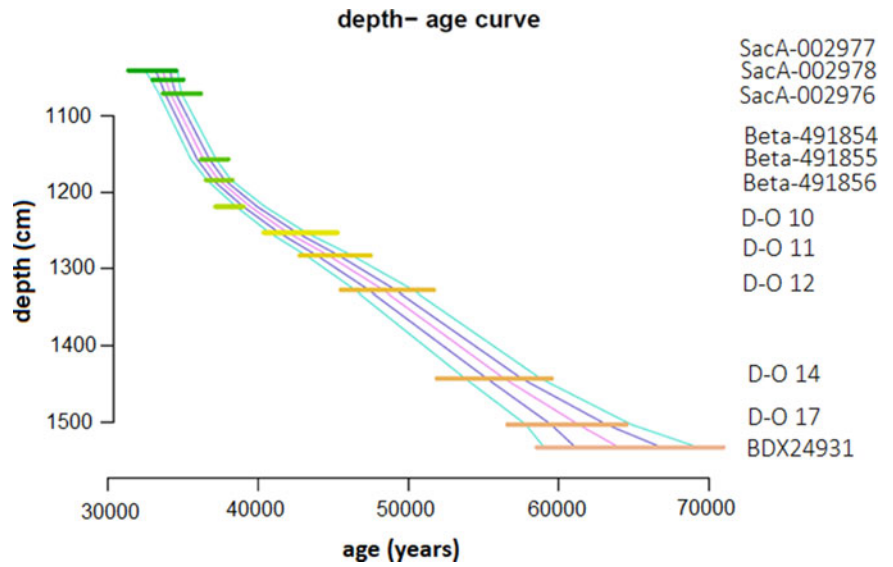


Figure 3. Depth-age model with Bayesian statistics using ChronoModel software and ArchaeoPhases package. Horizontal colored and thick lines represent the ages used to create the model and sample (Table 1); labels are represented on the right. The other colored lines, which cut the ages, are the calculated median age (pink) with two estimated probabilities at 68% (between the two purple lines) and 95% (green lines).

between 64.0–60.0 ka based on the combination of ¹⁴C and isotopic event stratigraphy (Sánchez Goñi et al., 2013). It is also younger compared to the age given by the Villars Cave speleothem (63.3–60.9 ± 0.8 ka; Genty et al., 2010). Moreover, GS 18, which would be the counterpart of HS 6 in Greenland, is dated at ca. 63.8–59.4 ka (Rasmussen et al., 2014). However, in our record, there is no evidence that the grains were not completely bleached. HS 6 is a climatic phase encompassing a large input of IRD, which may have resulted in reworking, but we need to further investigate

this hypothesis and increase the number of dated ages. This exploratory approach of dating marine sediments by luminescence and the preliminary pIR-IR₂₉₀ age seems promising, which obviously needs to be confirmed with other luminescence testing and the dating of younger HSs (HS 1–4) whose ages can be compared with those obtained with ¹⁴C in order to validate the analytical strategy adopted.

The age-depth curve constructed with ArchaeoPhases, according to the hierarchical Bayesian model in ChronoModel, gives

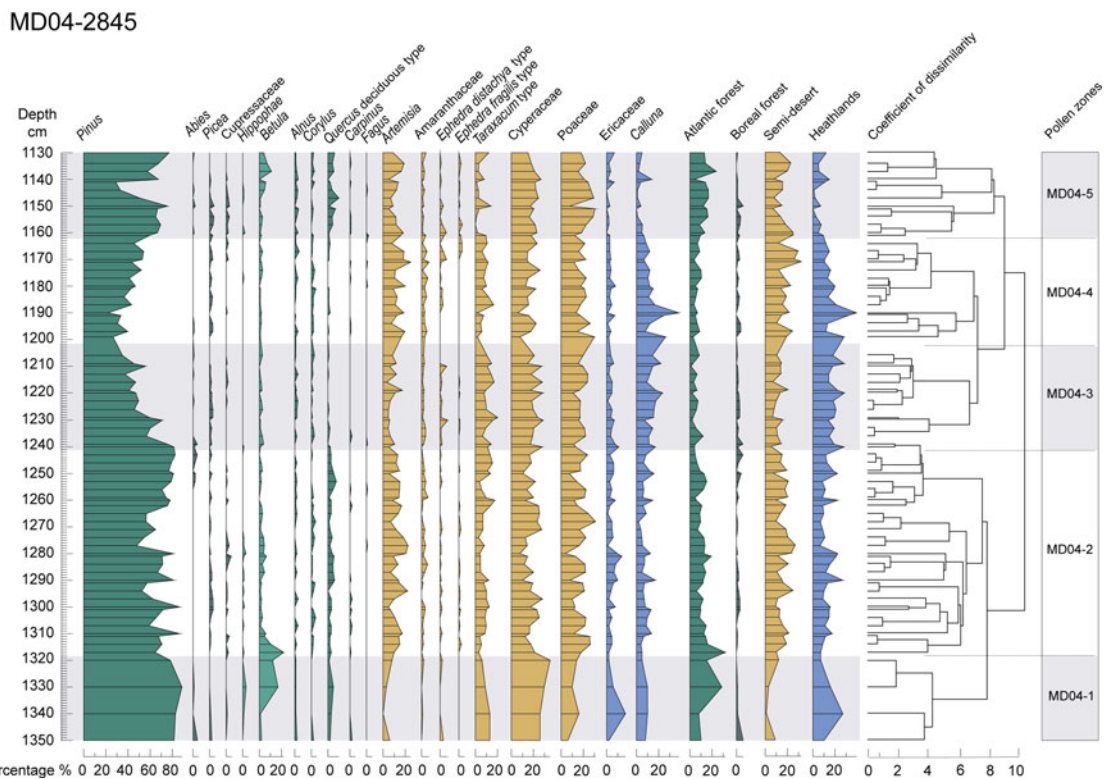


Figure 4. Pollen diagram of the MD04-2845 deep-sea core between 1335–1130 cm depth. From left to right: selected taxa, ecological groups (Atlantic forest, boreal forest, semi-desert plants, heathlands), and pollen zones, based on the clustering analysis and optical partitioning.

Table 4. ^{14}C dates of the three new samples and the other ^{14}C ages used in this study and their calibration with Calib v.8.2.

ID_laboratory	Depth (cm)	Material	pMC	$\delta^{13}\text{C}$ (‰)	AMS ^{14}C age (^{14}C ka BP)	Error (^{14}C ka BP)	Age Calib (2σ - cal BP)
SacA-002977	1048	<i>G. bulloides</i>	2.47 ± 0.12	-1.7	29.87	0.39	32.389–30.493
SacA-002978	1060	<i>N. pachyderma</i> (s)	2.19 ± 0.12	2.6	30.67	0.42	33.253–31.518
SacA-002976	1078	<i>G. bulloides</i>	2.02 ± 0.12	0.6	31.35	0.46	33.985–32.182
Beta - 491854	1164	<i>N. pachyderma</i> (s)	1.47 ± 0.04	0.3	33.92	0.22	36.173–34.731
Beta - 491855	1191	<i>N. pachyderma</i> (s)	1.57 ± 0.04	0.2	33.39	0.22	35.220–34.215
Beta - 491856	1226	<i>N. pachyderma</i> (s)	1.43 ± 0.04	0.5	34.14	0.23	36.557–34.982

information on sedimentation rate based on ages and uncertainties (Fig. 3). Although the ^{14}C and IRSL ages are younger, all the ages are slightly older in the depth-age model. This effect comes from the a priori stratigraphic constraint, which adjusts the ages by reducing uncertainties according to the stratigraphy of the sedimentary sequence. The sedimentation rate of the core is relatively constant from 70–40 ka, but it changes later on. The two dates around 1200 cm correspond to HS 4, which is marked by a different and rapid sedimentary process, such as an IRD deposition.

Vegetation and climate changes in SW France and its margin

Cluster analysis and broken-stick method applied to the pollen assemblage identified five pollen zones (MD04-1 to MD04-5), ranging from 1350–1130 cm deep (Fig. 4), ca. 49.8 ± 2.0 to 35.6 ± 0.8 ka (Fig. 6).

Zones MD04-1 and MD04-5 are characterized by an increase in the percentages of Atlantic forest taxa. The first zone (ca. 49.8–47.3 ka) is marked by a higher increase in temperate forest (29%) and, in particular, *Betula* (17%), *Hippophae* (3%), and deciduous *Quercus* (5%). Zone MD04-5 (ca. 36.7–35.6 ka) suggests a renewed forest expansion composed of *Betula*, Cupressaceae, deciduous *Quercus*, *Alnus*, *Corylus*, *Carpinus*, and *Fagus*, reflecting a warmer and wetter climate. Zone MD04-2 (ca. 47.3–40.9 ka) is characterized by steppe expansion, consisting of *Artemisia*, Amaranthaceae, Cyperaceae, and Poaceae, but also by forest expansion, as shown by increases of *Betula*, deciduous *Quercus*, *Alnus*, *Corylus*, and *Carpinus*. The boreal forest is

represented in zones MD04-3 (ca. 40.9–38.3 ka), which is marked by the highest percentage of *Abies* in the entire sequence (4%), reflecting a cooling. This zone is also marked by a significant increase in humidity and a cold climate, as reflected by percentages of *Calluna* (e.g., 22% at ca. 38.7 ± 0.8 ka, 1209 cm; 23% at ca. 39.4 ± 0.9 ka, 1220 cm). On the contrary, MD04-4 (ca. 38.3–36.7 ka) is characterized by an increase in steppe taxa (32% at ca. 36.9 ± 0.9 ka, 1170 cm), especially *Artemisia* (19%), Poaceae (30%), and Cyperaceae (23%), along with the presence of boreal forest (2% of *Picea*), indicating a colder and drier climate. The beginning of the zone is marked by an increase in the percentages of *Calluna* species (38% at ca. 37.7 ± 0.8/0.81 ka, 1190 cm) reflecting a cold and humid climate. In this zone, *E. fragilis* is virtually absent. Within this zone, the percentages of *Pinus* decrease slightly around 38.2 ± 0.8 ka (1200 cm).

The results of the PCA explain 45% of the variance. The PCA identifies a first component (Fig. 5), that explains 25.9% of the variance characterized by deciduous *Quercus* and *Betula* with positive scores (warm), and herbaceous and shrub taxa such as Ericaceae, *Calluna*, and Cyperaceae (cold) with negative scores. The second dimension, which explains 19% of the variance, is characterized by the positive scores of forest taxa, such as deciduous *Quercus* and *Betula*, and Ericaceae, which is a moist-loving taxon, while *Artemisia*, Poaceae, and Cyperaceae fall in the negative scores. In other words, variations of PC1 scores are used in this study as a warm/cold index and PC2 variations are used as a dry/wet and oceanic/continental proxy (Fig. 6E). Therefore, zones MD04-1 and MD04-5 represent relatively warm and wet climate, zones

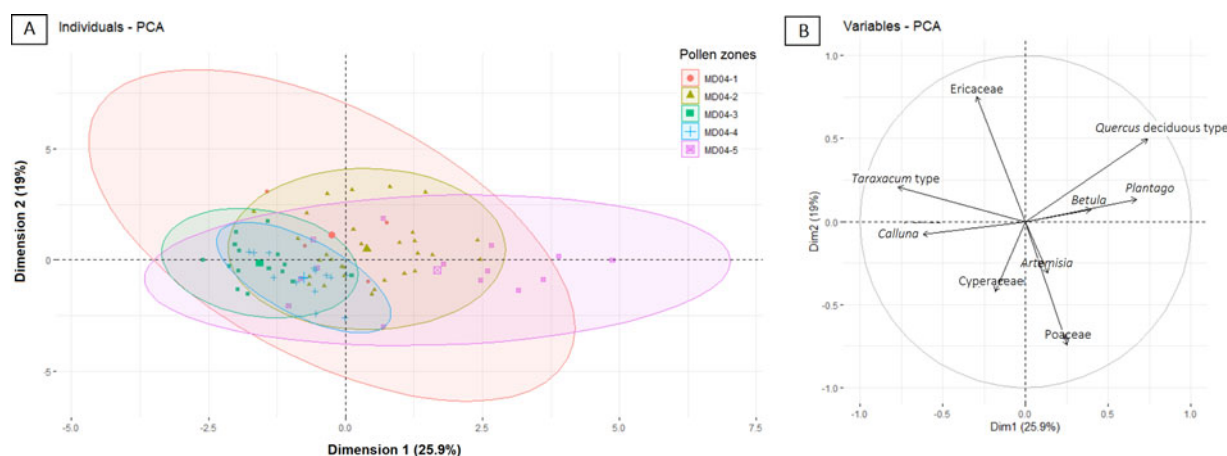


Figure 5. Principal Components Analysis (PCA) representing (a) pollen zones-based confidence ellipses, and (b) the 9 major taxa, with pollen percentages estimated to be >6% for at least 5 samples.

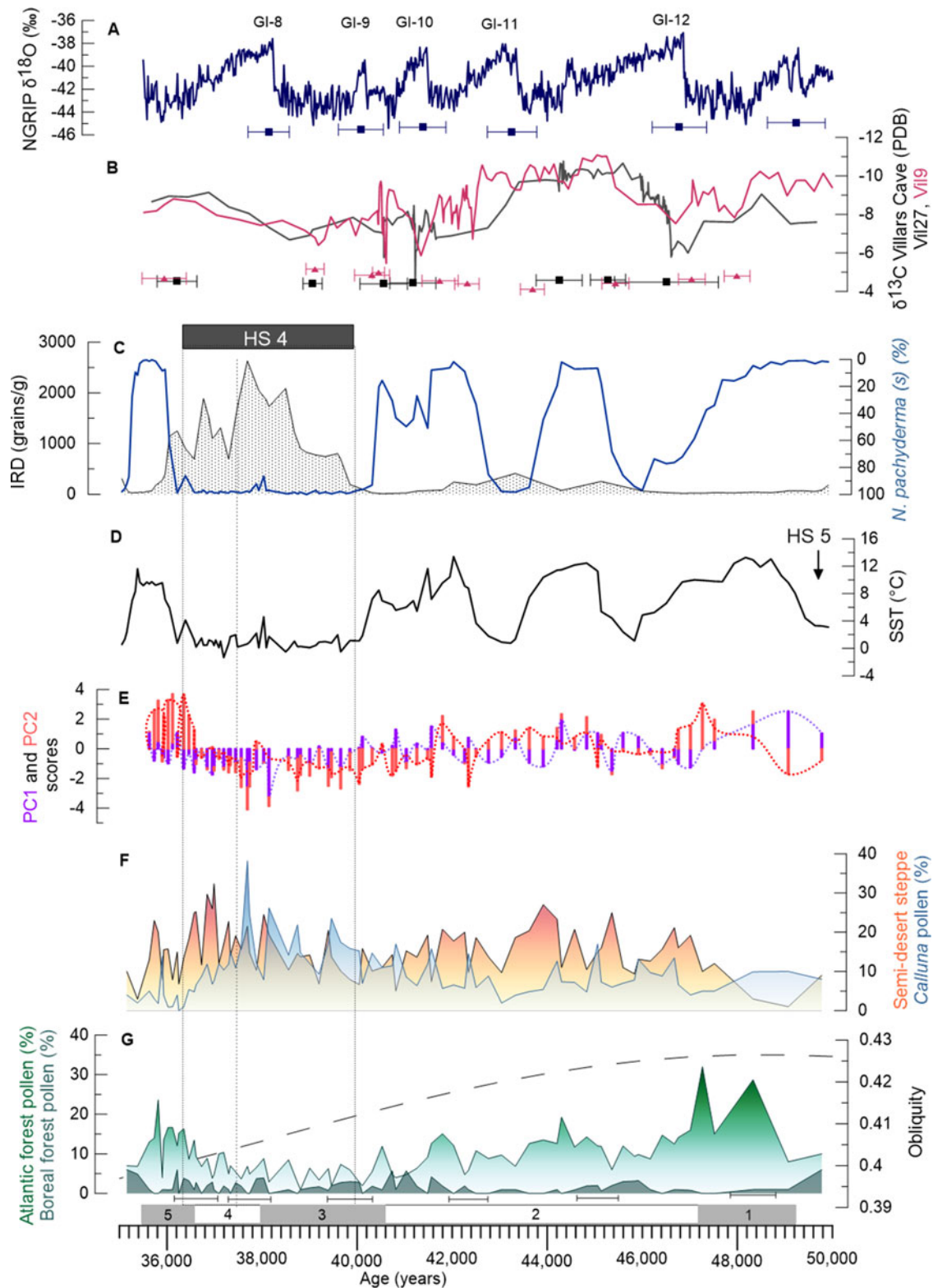


Figure 6. Oceanic and continental climatic multiproxies in the core, discussed from the bottom to the top of the figure. (F, G) Pollen percentages of Atlantic forest (degraded green), boreal forest (green), semi-desert plants (orange), *Calluna* (blue); obliquity curve (Laskar et al., 2004) is represented with the temperate and boreal forest (G). (E) PC1 (purple) and PC2 (red) scores are represented in two different forms: purple/red bar charts and purple/red dotted curves. Dim1 (=PC1): the negative values correspond to dryness and positive to cold environments and Dim2 (=PC2) with positive scores to warm and negative scores to humid taxa (D), the annual sea surface temperature of Bay of Biscay (SST) derived from the polar foraminiferan *Neogloboquadrina pachyderma* (s) percentages, and quantity of IRD (C). The percentage scale of *N. pachyderma* (s) is reversed with respect to IRD. Villars stalagmites $\delta^{13}\text{C}$ (B) VIL27 (gray) and VIL9 (red) and both of their chronological uncertainties are represented (only some uncertainties are shown; all uncertainties are available in Genty et al., 2003). (A) NorthGRIP $\delta^{18}\text{O}$ curve (Rasmussen et al., 2014) and the uncertainties for the GIs (Wolff et al., 2010). Dotted rectangle (C–G) represents HS 4; dashed line indicates the separation between the two climatic phases within HS 4.

MD04-3 and MD04-4 colder and drier than the previous ones, and MD04-2 represents a relatively cold and wet climate. The warm and humid terrestrial phases are associated with the highest SST in the Bay of Biscay (Fig. 6D). The cold and dry terrestrial phases (Fig. 6F) are synchronous with cold SST, while the cold and humid phase is associated with SST oscillations.

Clustering analysis recognizes 14 pollen zones. However, optimal partitioning that gives the statistical significance of the zones has only detected 5 pollen zones and, therefore, D-O variability is not recorded from pollen percentages. However, in pollen zone MD04-2, two small increases in forest percentages are associated with two large SST increases that correspond with D-O 11 and D-O 10. Therefore, this variability, which was undetected by the optimal partitioning, seems to be real.

The chronology of the Middle to Upper Paleolithic technocomplexes

The ensemble of age models performed for each of the 11 sites in SW Europe (Fig. 7D, SI) show that the Châtelperronian, represented in this study by five sites mostly from the Aquitaine basin (i.e., Bordes-Fitte, Les Cottés, La Quina aval, and La Ferrassie) and Labeko-Koba (Wood et al., 2014) in the Spanish Basque country (Fig. 7D) spans from ca. 44.5 ka to ca. 40.1 ka. The Châtelperronian at la Quina aval and La Ferrassie could be the oldest (ca. 44 ka). The youngest ending time of this LTC would be, taking all uncertainties into account, ca. 40.3 ka at Les Cottés and ca. 40.1 ka at La Ferrassie.

The Proto-Aurignacian, the first LTC attributed to the Upper Paleolithic and *Homo sapiens*, is found at Les Cottés, Isturitz (Barshay-Szmidt et al., 2018) and Gatzarria (Barshay-Szmidt et al., 2012) in the French Basque country, and at Labeko-Koba, Covalejos, and Cobrante in the Cantabrian of Spain (Marín-Arroyo et al., 2018). It could have developed between ca. 44.2–41.4 ka at Isturitz and between 42.3–40.4 ka at Gatzarria. In northern Spain, it appeared in Covalejos between ca. 41.9–40.0 ka, in Labeko-Koba ca. 41.3–40.8 ka, ca. 41.3–39.1 ka in Cobrante, and in El Cuco between ca. 41.1–39.0 ka. In SE France, the Proto-Aurignacian, which is represented in our model only by Esquicho-Grapaou (Barshay-Szmidt et al., 2020), spans between ca. 42.9–38.0 ka. The youngest Proto-Aurignacian starting time is found at the Les Cottés site, which is dated between ca. 40.6–39.6 ka. The Proto-Aurignacian would be present in Western Europe first in northern Spain, then in SE France and the Aquitaine basin. However, this hypothesis is based on only a few well-dated sites from SW Europe.

The Proto-Aurignacian chronologically overlaps with the Châtelperronian. In SW France, taking into account the oldest and the most recent age from the Les Cottés and La Ferrassie sites, the overlap spans ca. 500 years. However, according to the techno-cultural attribution at the Bordes-Fitte site, which has the oldest presence of an Aurignacian occupation, this overlap would be ca. 1,100 years. Farther south, in the Basque country and Cantabrian region, the Châtelperronian overlaps with the Proto-Aurignacian for ca. 1,800 years, if we accept that the chronology of Isturitz is sufficiently reliable.

The Early Aurignacian is stratigraphically above the Proto-Aurignacian. It is represented by six sites located in SW France, the French and Spanish Basque country, and northern Spain. The Early Aurignacian is the oldest north of the Aquitaine basin at the Bordes-Fitte site, 41.2–40.1 ka, and in the Basque country at Isturitz, ca. 40.8–40.0 ka. It could have developed at

Labeko-Koba between ca. 40.5–39.7 ka, and at Covalejos ca. 40.3–39.0 ka. In southwestern France, it appeared at Gatzarria between ca. 39.9–38.3 ka and ca. 39.4–38.8 ka at Les Cottés.

DISCUSSION

Climatic and environmental changes in SW France from GI 12–8 (ca. 50–36 ka)

The phases marked by the increase of Atlantic forest (Fig. 6G) are associated with the SST warming in the Bay of Biscay (Fig. 6C). Conversely, the phases dominated by semi-desert plants (Fig. 6F) are synchronous with cold SST. The chronologies of the four temperate phases punctuating the period between HS 5 and HS 4, does not correspond with the chronologies of GI 12–8, defined according to the Greenland $\delta^{18}\text{O}$ record (Fig. 6A) (Rasmussen et al., 2014). These SW European warming events show a difference of ca. 1,000 years from our age-depth model, compared to the onset of these GIs. This difference falls, however, within the uncertainties of the Greenland age model (800–1,300 years, Table 1) and the uncertainties of radiocarbon ages of this period. Atlantic forest pollen percentages indicate a progressive long-term decrease in the forest cover from GI 12–8, paralleling the decrease in obliquity (Fig. 6G), suggesting a warmer GI 12 (28%), compared to the other GIs. The high values of $\delta^{13}\text{C}$ from two stalagmites in the Villars Cave (Genty et al., 2010) further indicate an increase in precipitation during GI 12 (Fig. 6A, B).

During HS 4, the SST was strongly imprinted by *N. pachyderma* (s) percentages, which decreased a few centuries before the increase of IRD (Fig. 6C). SST in the Bay of Biscay probably cooled contemporaneously with the first IRD discharges in the more northwestern regions. Therefore, and following the previous work of Sánchez Goñi et al. (2000), we define the time period of HS 4 in the Bay of Biscay between ca. 40.2–36.5 ka by using collectively the decrease of SST and the increases of *N. pachyderma* (s) and IRD. The age of HS 4, which is estimated between 40.2–38.3 cal BP (Sanchez Goñi and Harrison, 2010), is based on the synthesis of ^{14}C ages from North Atlantic deep-sea cores made by Elliot et al. (2002). The timing of the end of HS 4 given by the Bayesian age-depth model in core MD04-2845 using the new ^{14}C age is ca. 1,500 years younger than that based on the North Atlantic ^{14}C . However, taking into account all the uncertainties, our new age-model does not fundamentally contradict the traditional chronology of HS 4.

In SW France, HS 4 is composed of two climatic phases (Fig. 6). This subdivision into two phases was detected previously in a core from the northwestern Iberian margin (MD99-2331, 42°9'N, 9°69'W; Naughton et al., 2009). Our first phase (ca. 40.2–37.5 ka) is marked by the strongest iceberg discharges and is contemporaneous with the decrease of the Atlantic forest and maximum percentages of *Calluna*. This genus is a moisture and light-demanding plant whose development is favored by forest contraction (Naughton et al., 2009), reflecting an increase in humidity. Sea surface temperatures drop by $\sim 7 \pm 5^\circ\text{C}$. A slowdown in the growth of the Villars Cave speleothems is recorded during HS 4, also indicating a drastic decrease in precipitation in this region (Genty et al., 2003). Our second phase of HS 4 (ca. 37.5–36.4 ka) is synchronous with a moderate amount of IRD compared to the first phase, but the maximum of *N. pachyderma* (s) maintained low SSTs, between $0\text{--}2 \pm 2^\circ\text{C}$ in the Bay of Biscay.

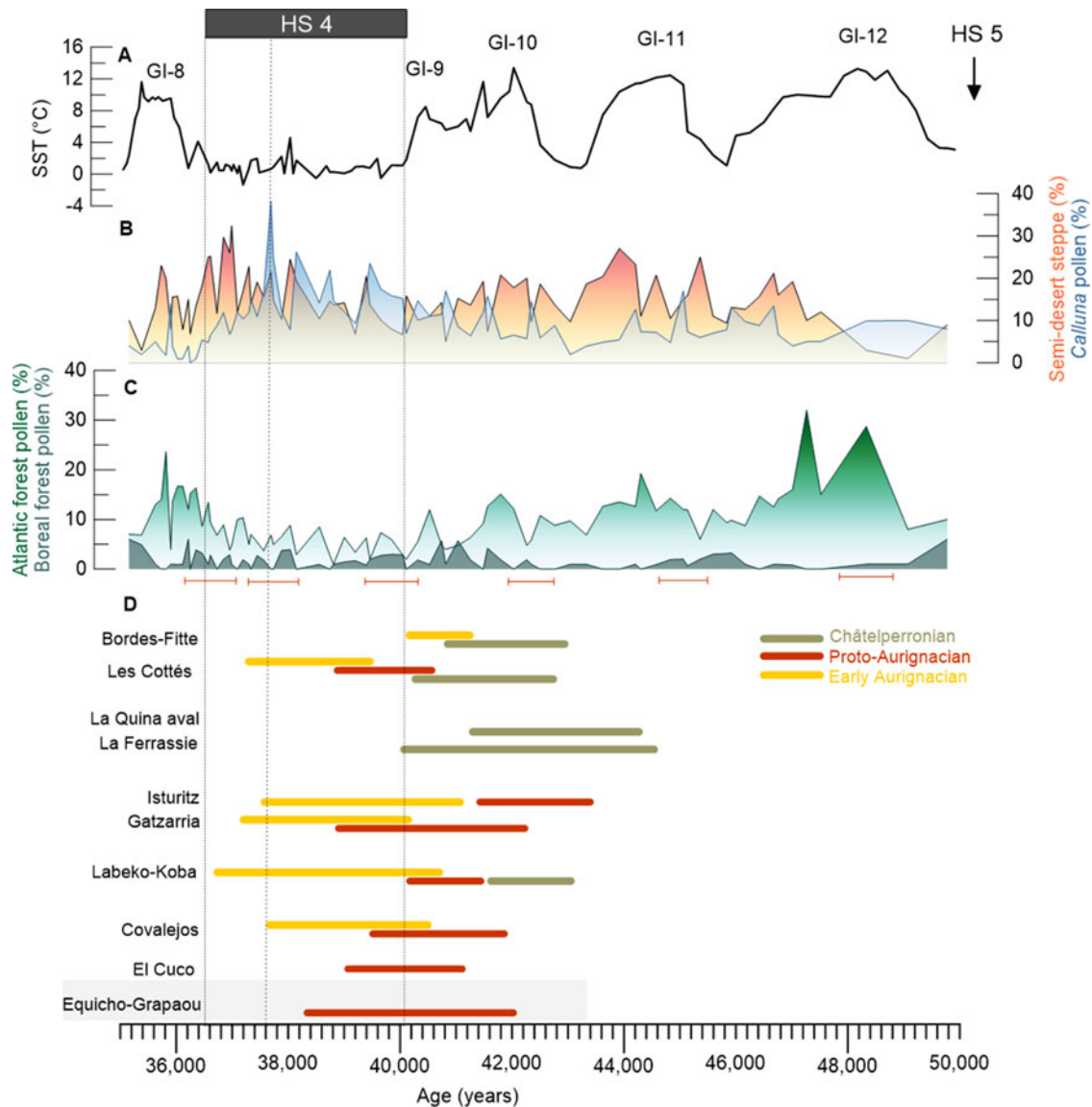


Figure 7. Comparison between environmental/climatic data and archaeological LTCs. (A) Bay of Biscay SST. (B, C) Pollen percentages of Atlantic forest (green), boreal forest (dark green), semi-desert steppe (orange), and *Calluna* species. (D) Representation of Middle to Upper Paleolithic transition LTCs. Modeled time ranges at 68.2% for Châtelperronian (green), Proto-Aurignacian (dark orange), and Early Aurignacian (yellow). The gray horizontal rectangle represents the only site of SE France. Dotted rectangle represents HS 4; dashed line indicates the separation between the two climatic phases within HS 4.

Interestingly, within the first phase, SST and *N. pachyderma* (s) indicate a slight warming of $2 \pm 3^\circ\text{C}$ towards 38.2 ± 0.9 ka, which is associated with a small decrease in IRD. The percentages of *N. pachyderma* (s) fall to a value of 86.4% and SST increases by $\sim 4 \pm 3^\circ\text{C}$. Another deep-sea core off the Iberian Peninsula (MD95-2039, $40^\circ 34'\text{N}$, $10^\circ 20'\text{W}$) shows a slight warming associated with an increase in deciduous *Quercus* (Roucoux et al., 2005), which could indicate regional warming in the middle of HS 4 between $40\text{--}45^\circ\text{N}$. In the Bay of Biscay, the percentage of deciduous *Quercus* (1%) remains low, but the Atlantic forest reaches almost 9% due to a 3% increase in *Alnus*, 2% in *Corylus*, and 1% in *Betula* and *Carpinus*.

HS 4 is thus divided into two different climatic and environmental phases in the eastern North Atlantic region between 40°N and 45°N : a first phase, associated with the maximum amount of IRD and marked by extreme cooling and wet conditions; and a second phase, characterized by a drier and colder climate showing

a warming trend. However, unlike the cores from the Iberian margin, where the first phase is considered to be the coldest one, the two phases in the Bay of Biscay are relatively similar in terms of forest cover and oceanic temperatures throughout HS 4.

Climatic and environmental changes: triggers for technological adaptations?

The studies of SW France archaeological sites played a major role in the definition of both Middle and Upper Paleolithic cultures. The oldest appearance of the Châtelperronian at la Quina aval and La Ferrassie (ca. 44 ka) could be contemporaneous with GS 11 (Fig. 7). The presence of Châtelperronian at La Ferrassie would be the earliest presence in SW France, well before the Châtelperronian from Arcy-sur-Cure (Talamo et al., 2020). Farther north, at Bordes-Fitte rockshelter and Les Cottés Cave, it might have begun between $42.9\text{--}41.5$ ka, corresponding perhaps

to the end of GS 11. At Labeko-Koba, the most southern site, the Châtelperronian is dated between 43.0–41.6 ka and encompasses the end of GS 11. Depending on the region, the Châtelperronian developed since the end of GS 11 or during GS 10. However, in SW France and northern Spain, the Châtelperronian does not appear beyond the beginning of HS 4. The last age of the Châtelperronian, which is associated with the last Neanderthals, indicates that their disappearance would have occurred in this region at the same time as the start of HS4.

The Proto-Aurignacian could have appeared in SW and SE France, as well as in northern Spain, around the GS 10/GS 9 transition, which is marked by the expansion of an open forest with steppe-like elements. Shao et al. (2021), using a global climate model, developed a human-existence model combining climate data with archaeological sites to reconstruct patterns of Aurignacian dispersal. The earliest Aurignacian dispersal in Europe started before 45 ka (Hublin et al., 2020). The recent discovery in Mandrin Cave (Rhône valley) of a tooth that belonged to *H. sapiens*, has highlighted its presence in Western Europe before 50 ka (Slimak et al., 2022).

In Proto-Aurignacian levels, reindeer dominates the faunal assemblages in Charentes and Périgord, while horses and Bovidae are dominant in the Pyrenees (Discamps et al., 2010; Soressi et al., 2010; Barshay-Szmidt et al., 2018). Around GS 9, steppe and, to a lesser extent, boreal forest could explain the strong presence of reindeer; bison, and horses in both regions. Progressive reduction of forest cover from GS 9 to HS 4 probably also had an effect on modern human migration (Badino et al., 2020). So far, our age modeling suggests that the appearance of *Homo sapiens* would have occurred first in SW France, with migration later in SE France, arriving in northern Spain at ca. 41.8 ka. However, Talamo et al. (2020), using another age-modeling approach (IntCal 13, Reimer et al., 2013, and OxCal, Ramsey, 2009) obtained an age for Isturitz that is younger than our model, and, in this case, *Homo sapiens* would have arrived in SE France before farther west. Their scenario is consistent with the recent dating of the Proto-Aurignacian at Mandrin Cave, the beginning of which is dated between 43.3–42.2 ka (Slimak et al., 2022).

The first occurrences of the Early Aurignacian happened during GS 9 and the onset of HS 4 in Gatzarria and Les Cottés. The Early Aurignacian persisted during the beginning of HS 4. The faunal record also indicates a dominance of open and cold environmental faunal species in the Early Aurignacian (Discamps et al., 2010). Interestingly, within this LTC, a geographical difference also seems to emerge between the north and south, which are dominated by reindeer and by horses and Bovidae, respectively (Barshay-Szmidt et al., 2018). Unfortunately, no pollen data exists documenting a difference in the vegetation between the north and the south of SW France and northern Spain. The transition between Proto-Aurignacian and Early Aurignacian would overlap GS 9 and the first phase of HS 4.

The overlap between Châtelperronian and Proto-Aurignacian could be ca. 3,300 years between SW France and northern Spain. This overlap suggests a coexistence of several millennia between Neanderthal and modern groups (Marín-Arroyo et al., 2018), and interbreeding between Neanderthals and ancestors of non-African modern humans (Green et al., 2010). In recent years, genetic studies show the coexistence of Neanderthals and *Homo sapiens* by admixture from Neanderthals into ancestors of present populations in several regions of the world (Green et al., 2010; Prüfer et al., 2014, 2021; Fu et al., 2015; Bokelmann

et al., 2019; Bergström et al., 2020) either through a single (Sankararaman et al., 2012; Bergström et al., 2020) or multiple episodes of gene flow (Prüfer et al., 2014; Vernot and Akey, 2015; Villanea and Schraiber, 2019; Hublin et al., 2020).

Western Europe experienced strong climate changes, which affected the environments and the food resources of Neanderthals and modern humans. So far, the archaeological records show that the transition between each of the LTCs between 44–36 ka encompassed several warming and cooling events, and that the same LTC is not synchronous throughout SW France and northern Spain. However, the late Neanderthal LTC seems to have developed in a moderately forested landscape, while modern humans developed in successively more open environments.

Comparison of both paleoclimatic and archaeological records aiming to detect potential synchronies is a complex process due to the age resolution and typo-technological definitions. Therefore, the chronology of the Middle-Upper Paleolithic transition is still not conclusive and needs to be improved by enlarging the database and pursuing the chronological modeling approach using Bayesian statistics.

Our study further suggests that the disappearance of Neanderthals does not seem to be directly related to climate-driven environmental changes, although the Châtelperronian ended in several sites before HS 4 onset. However, uncertainty in determining the age of HS 4 and the apparent young age of this event in this marine record reveal that there is an uncertainty making it difficult to assume a relationship between the end of the Châtelperronian and HS 4 onset. In SW France and the Cantabrian regions, the late Neanderthals survived several warming and cooling events, but just disappeared after the first LTCs associated with modern humans are recorded. Furthermore, the progressive increase of open environments from ca. 50–40 ka would have been favorable to expansion of modern humans, who could have been well adapted to the steppe. They could have competed with the late Neanderthals for the same ecological niches, causing their regional disappearance. Our new data are in line with previous modeling studies showing that Neanderthal disappearance can only be achieved when modern humans are chosen in the model as being more adapted in the exploitation of food resources and hunting technology compared to Neanderthals (Sepulchre et al., 2007; Banks et al., 2008; Columbu et al., 2020; Timmermann, 2020).

CONCLUSIONS

The high resolution pollen study of the MD04-2845 deep-sea core retrieved from the Bay of Biscay precisely identified the effect of climate changes from D-O 12–8 cycles and HS 4 in SW France. HS 4, defined on the basis of increases in IRD and *N. pachyderma* (s), is characterized by two distinct climatic phases: a first wet and cold phase and a second drier and colder phase. In the long term, a progressive decrease in the Atlantic forest and concomitant expansion of open environments is recorded from 50–40 ka. From a chronological point of view, IRSL dating results on the MD04-2845 deep-sea core seems promising, and future sample dating should confirm its application for sedimentary sequences older than the limits of radiocarbon dating. In addition, Bayesian statistics for both paleoclimatic and archaeological data from the westernmost part of Europe allowed us to improve the identification of potential synchronies. This critical work on an archaeological database and chronological modeling could be

applied to Mousterian (older) LTCs to better characterize their variability over the Middle Paleolithic.

This comparison shows that changes in LTCs during the Middle to Upper Paleolithic transition do not correspond with punctual vegetation and climate changes. In contrast, progressive opening of the regional landscape seems to have provided the context for the replacement of Neanderthals by modern humans, which lasted several millennia during which potential interbreeding and cultural changes occurred. Finally, our data suggest that climate changes did not directly cause the disappearance of Neanderthal. That disappearance was probably the result of competition with *Homo sapiens* for the same ecological niches.

Supplementary Material. The supplementary material for this article can be found at <https://doi.org/10.1017/qua.2022.21>

Acknowledgments. This work was initially funded by the New Aquitaine Region NATCH scientific project (*Neanderthalenses aquitanensis*: Territoires, Chronologie, Humanité, co-dir. J.Ph. Faivre, C. Lahaye, B. Maureille), and continued during a doctoral contract n°12-18 (Ecole Doctorale Montagne Humanités), and by financial support from the French Research National Agency under the Investissements d'Avenir Program (ANR-10-LABX-52). ¹⁴C dating was carried out with the support of ERC Advanced Grant TRACSYMBOLS no. 249587. We thank the members of UMR 5805 EPOC and UMR 6034 Archeosciences Bordeaux for their technical assistance (L. Devaux, M. Georget, M.-H. Castera, O. Thier, and I. Billy; J. Faure). Thanks to D. Genty and S. Salonen for their help and interesting discussions. We thank the three anonymous referees for their insightful comments to revise this paper.

REFERENCES

- Aitken, M.J., 1998. *An Introduction to Optical Dating: The Dating of Quaternary Sediments by the Use of Photon-stimulated Luminescence*. Oxford University Press, Oxford, New York.
- Allen, G., Castaing, P., 1977. Carte de répartition des sédiments superficiels sur le plateau continental du Golfe de Gascogne. *Bulletin de l'Institut de Géologie du Bassin d'Aquitaine* **23**, 255–260.
- Armitage, S.J., Pinder, R.C., 2017. Testing the applicability of optically stimulated luminescence dating to Ocean Drilling Program cores. *Quaternary Geochronology* **39**, 124–130.
- Badino, F., Pini, R., Ravazzi, C., Margaritora, D., Arrighi, S., Bortolini, E., Figus, et al., 2020. An overview of Alpine and Mediterranean paleogeography, terrestrial ecosystems and climate history during MIS 3 with focus on the Middle to Upper Palaeolithic transition. *Quaternary International* **551**, 7–28.
- Banks, W.E., d'Errico, F., Peterson, A.T., Kageyama, M., Sima, A., Sánchez-Goni, M.-F., 2008. Neanderthal extinction by competitive exclusion. *PLoS ONE* **3**, e3972. <https://doi.org/10.1371/journal.pone.0003972>.
- Banks, W.E., d'Errico, F., Zilhão, J., 2013. Human-climate interaction during the early Upper Paleolithic: testing the hypothesis of an adaptive shift between the Proto-Aurignacian and the Early Aurignacian. *Journal of Human Evolution* **64**, 39–55.
- Bard, E., Arnold, M., Mangerud, J., Paterne, M., Labeyrie, L., Duprat, J., Mélières, M.-A., Sonstegaard, E., Duplessy, J.-C., 1994. The North Atlantic atmosphere-sea surface ¹⁴C gradient during the Younger Dryas climatic event. *Earth and Planetary Science Letters* **126**, 275–287.
- Barshay-Szmidt, C.C., Eizenberg, L., Deschamps, M., 2012. Radiocarbon (AMS) dating the Classic Aurignacian, Proto-Aurignacian and Vasconian Mousterian at Gatzarria Cave (Pyrénées-Atlantiques, France). *PALEO Revue d'Archéologie Préhistorique* **23**, 11–38.
- Barshay-Szmidt, C., Normand, C., Flas, D., Soulier, M.-C., 2018. Radiocarbon dating the Aurignacian sequence at Isturitz (France): Implications for the timing and development of the Protoaurignacian and Early Aurignacian in western Europe. *Journal of Archaeological Science: Reports* **17**, 809–838.
- Barshay-Szmidt, C., Bazile, F., Brugal, J.-P., 2020. First AMS ¹⁴C dates on the Protoaurignacian in Mediterranean France: The site of Esquicho-Grapaou (Russan-Ste-Anastasie, Gard). *Journal of Archaeological Science: Reports* **33**, 102474. <https://doi.org/10.1016/j.jasrep.2017.09.003>.
- Bartolomei, G., Broglio, A., Cassoli, P.F., Castelletti, L., Cattani, L., Cremaschi, M., Giacobini, G., et al., 1994. La Grotte de Fumane. Un site aurignacien au pied des Alpes. *Preistoria Alpina* **28**, 131–179.
- Bateman, M.D., Swift, D.A., Piotrowski, J.A., Rhodes, E.J., Damsgaard, A., 2018. Can glacial shearing of sediment reset the signal used for luminescence dating? *Geomorphology* **306**, 90–101.
- Bateman, M.D., Swift, D.A., Piotrowski, J.A., Sanderson, D.C.W., 2012. Investigating the effects of glacial shearing of sediment on luminescence. *Quaternary Geochronology* **10**, 230–236.
- Bazile, F., 1977. Nouvelles données sur le Paléolithique Supérieur ancien en Languedoc Oriental. *20th Congrès Préhistorique de France, Provence, 1974, Châteauneuf-les-Martigues*. SPF, Paris, pp. 24–28.
- Berger, J.-F., Guilaine, J., 2009. The 8200 cal BP abrupt environmental change and the Neolithic transition: a Mediterranean perspective. *Quaternary International* **200**, 31–49.
- Bergström, A., McCarthy, S.A., Hui, R., Almarri, M.A., Ayub, Q., Danecek, P., Chen, Y., et al., 2020. Insights into human genetic variation and population history from 929 diverse genomes. *Science* **367**, eaay5012. <https://doi.org/10.1126/science.aay5012>.
- Blaauw, M., Christen, J.A., 2011. Flexible paleoclimate age-depth models using an autoregressive gamma process. *Bayesian Analysis* **6**, 457–474.
- Bokelmann, L., Hajdinjak, M., Peyrégne, S., Brace, S., Essel, E., Filippo, C. de, Glocke, I., et al., 2019. A genetic analysis of the Gibraltar Neanderthals. *PNAS* **116**, 15610–15615.
- Bon, F., 2002. A brief overview of Aurignacian cultures in the context of the industries of the transition from the Middle to the Upper Paleolithic. In: Bar-Yosef, O., Zilhão, J. (Eds.), *Towards a Definition of the Aurignacian*. Trabalhos de Arqueologia 45, Lisboa, American School of Prehistoric Research/Instituto Português de Arqueologia, pp. 133–144.
- Bond, G., Lotti, R., 1995. Iceberg discharges into the North Atlantic on millennial timescales during the last glaciation. *Science* **267**, 1005–1010.
- Borrell, F., Junno, A., Barceló, J.A., 2015. Synchronous environmental and cultural change in the emergence of agricultural economies 10,000 years ago in the Levant. *PLoS ONE* **10**, e0134810. <https://doi.org/10.1371/journal.pone.0134810>.
- Brocheray, S., 2015. *Transferts et Accumulations sur les Marges du Golfe de Gascogne: Architecture, Fonctionnement et Contrôles*. These de doctorat, Océanographie, Université de Bordeaux, France.
- Brocheray, S., Cremer, M., Zaragosi, S., Schmidt, S., Eynaud, F., Rossignol, L., Gillet, H., 2014. 2000 years of frequent turbidite activity in the Capbreton Canyon (Bay of Biscay). *Marine Geology* **347**, 136–152.
- Broecker, W.S., Olson, E.A., 1961. Lamont radiocarbon measurements VIII. *Radiocarbon* **3**, 176–204.
- Butzin, M., Heaton, T.J., Köhler, P., Lohmann, G., 2020. A short note on marine reservoir age simulations used in IntCal20. *Radiocarbon* **62**, 865–871.
- Buylaert, J.-P., Jain, M., Murray, A.S., Thomsen, K.J., Thiel, C., Sohbat, R., 2012. A robust feldspar luminescence dating method for Middle and Late Pleistocene sediments. *Boreas* **41**, 435–451.
- Castaing, P., 1981. *Le Transfert à l'Océan des Suspensions Estuariennes: Cas de la Gironde*. Institut de géologie du Bassin d'Aquitaine, Bordeaux 1, Bordeaux, 530 pp.
- Castaing, P., Froidefond, J.-M., Lazure, P., Weber, O., Prud'homme, R., Jouanneau, J.-M., 1999. Relationship between hydrology and seasonal distribution of suspended sediments on the continental shelf of the Bay of Biscay. *Deep-Sea Research II* **46**, 1979–2001.
- Colas, F., 2003. *Circulation et Dispersion Lagrangiennes en Atlantique Nord-est*. Ph.D. dissertation, Université de Bretagne Occidentale, Brest, 253 pp.
- Columbu, A., Chiarini, V., Spötl, C., Benazzi, S., Hellstrom, J., Cheng, H., De Waele, J., 2020. Speleothem record attests to stable environmental conditions during Neanderthal–modern human turnover in southern Italy. *Nature Ecology & Evolution* **4**, 1188–1195.

- Correa-Metrio, A., Urrego, D.H., Cabrera, K.R., Bush, M.B., 2012. *paleoMAS. Paleoecological Analysis, R package version 2.0-1*. Vienna, The R Project for Statistical Computing, available at <<http://CRAN.R-project.org/package=paleoMAS>>
- Daniau, A.-L., Sánchez Goñi, M.F., Duprat, J., 2009. Last glacial fire regime variability in western France inferred from microcharcoal preserved in core MD04-2845, Bay of Biscay. *Quaternary Research* **71**, 385–396.
- Dansgaard, W., Johnsen, S., Clausen, H., Dahljensen, D., Gundestrup, N., Hammer, C., Oeschger, H., 1984. Evidence for general instability of past climate from a 250-kyr ice-core record. In: Hansen, J.E., Takahashi, T. (Eds.), *Climate Processes and Climate Sensitivity*. American Geophysical Union, Washington, DC.
- Dansgaard, W., Johnsen, S.J., Clausen, H.B., Dahl-Jensen, D., Gundestrup, N.S., Hammer, C.U., Hvidberg, C.S., et al., 1993. Evidence for general instability of past climate from a 250-kyr ice-core record. *Nature* **364**, 218–220.
- Dayet, L., d'Errico, F., Garcia-Moreno, R., 2014. Searching for consistencies in Châtelperronian pigment use. *Journal of Archaeological Science* **44**, 180–193.
- Defleur, A.R., Desclaux, E., Jabbour, R.S., Richards, G.D., 2020. The Eemian: global warming, ecosystem upheaval, demographic collapse and cannibalism at Moula-Guercy. A reply to Slimak and Nicholson (2020). *Journal of Archaeological Science* **117**, 105113. <https://doi.org/10.1016/j.jas.2020.105113>.
- d'Errico, F., Sánchez Goñi, M.F., 2003. Neandertal extinction and the millennial scale climatic variability of OIS 3. *Quaternary Science Reviews* **22**, 769–788. [https://doi.org/10.1016/S0277-3791\(03\)00009-X](https://doi.org/10.1016/S0277-3791(03)00009-X)
- d'Errico, F., Julien, M., Liolios, D., Vanhaeren, M., Baffier, D., 2003. Many awls in our argument. Bone tool manufacture and use in the Châtelperronian and Aurignacian levels of the Grotte du Renne at Arcy-sur-Cure. In: Zilhão, J., d'Errico, F. (Eds.), *The Chronology of the Aurignacian and of the Transitional Technocomplexes*. Dating, Stratigraphies, Cultural Implications. Instituto Portugues de Arqueologia, Lisbon, pp. 247–270.
- Discamps, E., Jaubert, J., Bachelier, F., 2011. Human choices and environmental constraints: deciphering the variability of large game procurement from Mousterian to Aurignacian times (MIS 5–3) in southwestern France. *Quaternary Science Reviews* **30**, 2755–2775.
- Discamps, E., Royer, A., 2017. Reconstructing palaeoenvironmental conditions faced by Mousterian hunters during MIS 5 to 3 in southwestern France: A multi-scale approach using data from large and small mammal communities. *Quaternary International* **433**, 64–87.
- Discamps, E., Soulier, M.-C., Bachelier, F., Bordes, J.-G., Castel, J.-C., Morin, E., 2010. Des faunes et des hommes: interactions entre environnements et cultures à la fin du Paléolithique moyen et au début du Paléolithique supérieur dans le Sud-Ouest de la France. In: Thiébaud, C., Costamagno, S., Claud, E. (Eds.), *Transitions, Ruptures et Continuité en Préhistoire*. XXVIIe Congrès Préhistorique de France—Bordeaux-Les Eyzies, 31 Mai–5 Juin 2010: Mémoires de la SPFÉditeurs, pp. 299–314
- Duller, G.A.T., 2015. The Analyst software package for luminescence data: overview and recent improvements. *Ancient TL* **33**, 35–42.
- Elliot, M., Labeyrie, L., Bond, G., Cortijo, E., Turon, J.-L., Tisnerat, N., Duplessy, J.-C., 1998. Millennial-scale iceberg discharges in the Irminger Basin during the Last Glacial Period: relationship with the Heinrich events and environmental settings. *Paleoceanography* **13**, 433–446.
- Elliot, M., Labeyrie, L., Dokken, T., Manthé, S., 2001. Coherent patterns of ice-rafted debris deposits in the Nordic regions during the last glacial (10–60 ka). *Earth and Planetary Science Letters* **194**, 151–163.
- Elliot, M., Labeyrie, L., Duplessy, J.-C., 2002. Changes in North Atlantic deep-water formation associated with the Dansgaard–Oeschger temperature oscillations (60–10ka). *Quaternary Science Reviews* **21**, 1153–1165.
- Feser, F., Barcikowska, M., Krueger, O., Schenk, F., Weisse, R., Xia, L., 2015. Storminess over the North Atlantic and northwestern Europe—a review. *Quarterly Journal of the Royal Meteorological Society* **141**, 350–382.
- Finlayson, C., Carrión, J.S., 2007. Rapid ecological turnover and its impact on Neandertal and other human populations. *Trends in Ecology & Evolution* **22**, 213–222.
- Fletcher, W.J., Sánchez Goñi, M.F., Allen, J.R.M., Cheddadi, R., Combourieu-Nebout, N., Huntley, B., Lawson, I., et al., 2010. Millennial-scale variability during the last glacial in vegetation records from Europe. *Quaternary Science Reviews* **29**, 2839–2864.
- Froidefond, J.-M., Castaing, P., Jouanneau, J.-M., 1996. Distribution of suspended matter in a coastal upwelling area. Satellite data and in situ measurements. *Journal of Marine Systems* **8**, 91–105.
- Fu, Q., Hajdinjak, M., Moldovan, O.T., Constantin, S., Mallick, S., Skoglund, P., Patterson, N., et al., 2015. An early modern human from Romania with a recent Neandertal ancestor. *Nature* **524**, 216–219.
- Galbraith, R.F., Roberts, R.G., Laslett, G.M., Yoshida, H., Olley, J.M., 1999. Optical dating of single and multiple grains from Jinmium rock shelter, Northern Australia: Part I, experimental design and statistical models. *Archaeometry* **41**, 339–364.
- Genty, D., Blamart, D., Ouahdi, R., Gilmour, M., Baker, A., Jouzel, J., Van-Exter, S., 2003. Precise dating of Dansgaard-Oeschger climate oscillations in western Europe from stalagmite data. *Nature* **421**, 833–837.
- Genty, D., Combourieu-Nebout, N., Peyron, O., Blamart, D., Wainer, K., Mansuri, F., Ghaleb, B., et al., 2010. Isotopic characterization of rapid climatic events during OIS3 and OIS4 in Villars Cave stalagmites (SW-France) and correlation with Atlantic and Mediterranean pollen records. *Quaternary Science Reviews* **29**, 2799–2820.
- Gilpin, W., Feldman, M.W., Aoki, K., 2016. An ecocultural model predicts Neandertal extinction through competition with modern humans. *PNAS* **113**, 2134–2139.
- Golovanova, L.V., Doronichev, V.B., Cleghorn, N.E., Koulikova, M.A., Sapelko, T.V., Shackley, M.S., 2010. Significance of ecological factors in the Middle to Upper Paleolithic transition. *Current Anthropology* **51**, 655–691.
- Gravina, B., Bachelier, F., Caux, S., Discamps, E., Favre, J.-P., Galland, A., Michel, A., Teyssandier, N., Bordes, J.-G., 2018. No reliable evidence for a Neandertal–Châtelperronian association at La Roche-à-Pierrot, Saint-Césaire. *Scientific Reports* **8**, 15134. <https://doi.org/10.1038/s41598-018-33084-9>.
- Green, R.E., Krause, J., Briggs, A.W., Maricic, T., Stenzel, U., Kircher, M., Patterson, N., et al., 2010. A draft sequence of the Neandertal genome. *Science* **328**, 710–722.
- Greenbaum, G., Friesem, D.E., Hovers, E., Feldman, M.W., Kolodny, O., 2019. Was inter-population connectivity of Neandertals and modern humans the driver of the Upper Paleolithic transition rather than its product? *Quaternary Science Reviews* **217**, 316–329.
- Grimm, E.C., 1987. A Fortran77 program for stratigraphically constrained cluster analysis by the method of incremental sum of squares. *Computers & Geosciences* **13**, 13–35.
- Guérin, G., Christophe, C., Philippe, A., Murray, A.S., Thomsen, K.J., Tribolo, C., Urbanova, P., et al., 2017. Absorbed dose, equivalent dose, measured dose rates, and implications for OSL age estimates: introducing the Average Dose Model. *Quaternary Geochronology* **41**, 163–173.
- Guibert, P., Schvoerer, M., 1991. TL dating: low background gamma spectrometry as a tool for the determination of the annual dose. *International Journal of Radiation Applications and Instrumentation. Part D. Nuclear Tracks and Radiation Measurements* **18**, 231–238.
- Guibert, P., Bechtel, F., Bourguignon, L., Lenoir, M., Brenet, M., Couchoud, I., Delagnes, A., et al., 2008. Une base de données pour la chronologie du paléolithique moyen dans le Sud-Ouest de la France. *Bulletin de la Société Préhistorique Française* **47**, 19–40.
- Hansen, V., Murray, A., Buylaert, J.-P., Yeo, E.-Y., Thomsen, K., 2015. A new irradiated quartz for beta source calibration. In: Bailiff, I.K., Chen, R., Duller, G.A.T., Huot, S., Lamothe, M. (Eds.), 14th International Conference on Luminescence and Electron Spin Resonance Dating, 7–11 July, 2014, Montréal, Canada. *Radiation Measurements* **81**, 123–127.
- Heaton, T.J., Köhler, P., Butzin, M., Bard, E., Reimer, R.W., Austin, W.E.N., Ramsey, C.B., et al., 2020. Marine20—the marine radiocarbon age calibration curve (0–55,000 cal BP). *Radiocarbon* **62**, 779–820.
- Heusser, L., Balsam, W.L., 1977. Pollen distribution in the northeast Pacific Ocean. *Quaternary Research* **7**, 45–62.

- Higham, T., Jacobi, R., Julien, M., David, F., Basell, L., Wood, R., Davies, W., Ramsey, C.B., 2010. Chronology of the Grotte du Renne (France) and implications for the context of ornaments and human remains within the Chatelperronian. *Proceedings of the National Academy of Sciences* **107**, 20234–20239.
- Hodgkins, J., Marean, C.W., Turq, A., Sandgathe, D., McPherron, S.J.P., Dibble, H., 2016. Climate-mediated shifts in Neandertal subsistence behaviors at Pech de l’Azé IV and Roc de Marsal (Dordogne Valley, France). *Journal of Human Evolution* **96**, 1–18.
- Hublin, J.-J., Talamo, S., Julien, M., David, F., Connet, N., Bodu, P., Vandermeersch, B., Richards, M.P., 2012. Radiocarbon dates from the Grotte du Renne and Saint-Césaire support a Neandertal origin for the Châtelperronian. *PNAS* **109**, 18743–18748.
- Hublin, J.-J., Sirakov, N., Aldeias, V., Bailey, S., Bard, E., Delvigne, V., Enderova, E., et al., 2020. Initial Upper Palaeolithic *Homo sapiens* from Bacho Kiro Cave, Bulgaria. *Nature* **581**, 299–302.
- Huntley, D.J., Baril, M.R., 1997. The K content of the K-feldspars being measured in optical dating or in thermoluminescence dating. *Ancient TL* **15**, 11–13.
- Hurrell, J.W., 1995. Decadal trends in the North Atlantic oscillation: Regional temperatures and precipitation. *Science* **269**, 676–679.
- Husson, F., Lê, S., Pagès, J., 2017. *Exploratory Multivariate Analysis by Example Using R*. Chapman and Hall/CRC, New York, 262 pp.
- Jaubert, J., 2011. Les archéo-séquences du Paléolithique moyen du Sud-Ouest de la France: Quel bilan un quart de siècle après François Bordes? *François Bordes et la Préhistoire, Éditions du Comité des Travaux Historiques et Scientifiques, Bordeaux*, pp. 235–253.
- Jaubert, J., Bordes, J.-G., Discamps, E., Gravina, B., 2011. A New Look at the end of the Middle Palaeolithic sequence in southwestern France. In: Derevianko, A.P., Shunkov, M.V. (Eds.) *Characteristic Features of the Middle to Upper Paleolithic Transition in Eurasia*. Novosibirsk, Asian Palaeolithic Association, pp. 102–115.
- Jouanneau, J.-M., Weber, O., Cremer, M., Castaing, P., 1999. Fine-grained sediment budget on the continental margin of the Bay of Biscay. *Deep-Sea Research II* **46**, 2205–2220.
- Juggins, S., 2019. rioja: Analysis of Quaternary Science Data. R package version 0.9-26. <https://cran.r-project.org/package=rioja>.
- Kars, R.H., Busschers, F.S., Wallinga, J., 2012. Validating post IR-IRSL dating on K-feldspars through comparison with quartz OSL ages. *Quaternary Geochronology* **12**, 74–86.
- Kassambara, A., Mundt, F., 2020. *factoextra: Extract and Visualize the Results of Multivariate Data Analyses. R Package Version 1.0.7*. <https://CRAN.R-project.org/package=factoextra>.
- Klingebl, A., Legigan, P., 1978. Histoire géologique des divagations de l’Adour. In: *Proceedings Congress IVème Centenaire du Détournement de l’Adour 1578–1978*. Bayonne Société des Sciences, Lettres et Arts de Bayonne, pp. 23–33.
- Kuehl, S.A., Nittrouer, C.A., Allison, M.A., Faria, L.E.C., Dukat, D.A., Jaeger, J.M., Pacioni, T.D., Figueiredo, A.G., Underkoffler, E.C., 1996. Sediment deposition, accumulation, and seabed dynamics in an energetic fine-grained coastal environment. *Continental Shelf Research* **16**, 787–815.
- Lanos, P., Dufresne, P., 2019. *ChronoModel version 2.0: Software for Chronological Modelling of Archaeological Data using Bayesian Statistics*, 2.0 ed.
- Lanos, P., Philippe, A., 2018. Event date model: a robust Bayesian tool for chronology building. *Communications for Statistical Applications and Methods* **25**, 131–157.
- Lapierre, F., 1967. Etude de la répartition des sédiments dans le Golge de Gascogne. *Institute Geologie Bassin Aquitaine Bulletin* **3**, 93–126.
- Laplace, G., 1966. Les Niveaux Castelperronien, Protoaurignacien et Aurignacien de la Grotte Gatzarria à Suhare en Pays Basque:(Fouilles 1961–1963). *Quartär-Internationales Jahrbuch zur Erforschung des Eiszeitalters und der Steinzeit* **17**, 117–140.
- Lascau, I., Feinberg, J.M., Dorale, J.A., Cheng, H., Edwards, R.L., 2016. Age of the Laschamp excursion determined by U-Th dating of a speleothem geomagnetic record from North America. *Geology* **44**, 139–142.
- Laskar, J., Robutel, P., Joutel, F., Gastineau, M., Correia, A.C.M., Levrard, B., 2004. A long-term numerical solution for the insolation quantities of the Earth. *Astronomy & Astrophysics* **428**, 261–285.
- Lavin, A., Valdes, L., Sanchez, F., Abaunza, P., Forest, A., Boucher, J., Lazure, P., Jegou, A.-M., 2006. Chapter 24. The Bay of Biscay: the encountering of the ocean and the shelf (18b,E). In: Robinson, A.R., Brink, K.H. (Eds.), *The Sea*. Harvard University Press, pp. 933–1001.
- Legendre, P., Gallagher, E., 2001. Ecologically meaningful transformations for ordination of species. *Oecologia* **129**, 271–280.
- Lowick, S.E., Trauerstein, M., Preusser, F., 2012. Testing the application of post IR-IRSL dating to fine grain waterlain sediments. *Quaternary Geochronology* **8**, 33–40.
- Mangerud, J., Bondevik, S., Gulliksen, S., Karin Hufthammer, A., Høisæter, T., 2006. Marine 14C reservoir ages for 19th century whales and molluscs from the North Atlantic. In: Rose, J., Tzedakis, P., Elderfield, H. (Eds.), Special Issue, Critical Quaternary Stratigraphy. *Quaternary Science Reviews* **25**, 3228–3245.
- Marín-Arroyo, A.B., Rios-Garaizar, J., Straus, L.G., Jones, J.R., Rasilla, M. de la, Morales, M.R.G., Richards, M., Altuna, J., Mariezkurrena, K., Ocio, D., 2018. Chronological reassessment of the Middle to Upper Paleolithic transition and early Upper Paleolithic cultures in Cantabrian Spain. *PLoS ONE* **13**, e0194708. <https://doi.org/10.1371/journal.pone.0194708>.
- Maroto, J., Soler, N., Fullola, J., 1996. Cultural change between Middle and Upper Paleolithic in Catalonia. In: Vaquero, M., Carbonell, E. (Eds.), *The Last Neandertals, the First Anatomically Modern Humans: A Tale About Diversity, Cultural Change and Human Evolution: the Crisis of 40 ka BP*. Universitat Rovira i Virgili; Capellades, Spain, pp. 219–250.
- Mary, Y., Eynaud, F., Colin, C., Rossignol, L., Brocheray, S., Mojtahid, M., Garcia, J., Peral, M., Howa, H., Zaragosi, S., Cremer, M., 2017. Changes in Holocene meridional circulation and poleward Atlantic flow: the Bay of Biscay as a nodal point. *Climate of the Past* **13**, 201–216.
- Mazières, A., Gillet, H., Castelle, B., Mulder, T., Guyot, C., Garlan, T., Mallet, C., 2014. High-resolution morphobathymetric analysis and evolution of Capbreton submarine canyon head (Southeast Bay of Biscay—French Atlantic Coast) over the last decade using descriptive and numerical modeling. *Marine Geology* **351**, 1–12.
- Mellars, P., 2004. Neanderthals and the modern human colonization of Europe. *Nature* **432**, 461–465.
- Monge Soares, A.M., 1993. The 14C content of marine shells: evidence for variability in coastal upwelling off Portugal during the Holocene. In: IAEA, *Isotope Techniques in the Study of Past and Current Environmental Changes in the Hydrosphere and the Atmosphere*. International Atomic Energy Agency (IAEA), Proceedings Series, pp. 471–485.
- Moss, P.T., Kershaw, A.P., 2007. A late Quaternary marine palynological record (oxygen isotope stages 1 to 7) for the humid tropics of northeastern Australia based on ODP Site 820. In: Kershaw, A.P., Haberle, S.G., Turney, C.S.M., Sophie C., Bretherton, S.C. (Eds.), Special Issue, Environmental History of the Humid Tropics region of north-east Australia. *Palaeogeography, Palaeoclimatology, Palaeoecology* **251**, 4–22.
- Murray, A.S., Wintle, A.G., 2003. The single aliquot regenerative dose protocol: potential for improvements in reliability. In: McKeever, S.W.S. (Ed.), Special Issue, Proceedings of the 10th International Conference on Luminescence and Electron-Spin Resonance Dating (LED 2002). *Radiation Measurements* **37**, 377–381.
- Naughton, F., Sánchez Goñi, M.F., Kageyama, M., Bard, E., Duprat, J., Cortijo, E., Desprat, S., et al., 2009. Wet to dry climatic trend in north-western Iberia within Heinrich events. *Earth and Planetary Science Letters* **284**, 329–342.
- Nelson, M., Rittenour, T., Cornachione, H., 2019. Sampling Methods for Luminescence Dating of Subsurface Deposits from Cores. *Methods and Protocols* **2**, 88. <https://doi.org/10.3390/mps2040088>.
- Ning, S., Dupont, L.M., 1997. Vegetation and climatic history of southwest Africa: A marine palynological record of the last 300,000 years. *Vegetation History and Archaeobotany* **6**, 117–131.
- Normand, C., Turq, A., 2005. L’Aurignacien de la grotte d’Isturitz (France): la production lamellaire dans la séquence de la salle de Saint-Martin. In: Le Brun-Ricalens, F. (Dir.), *Productions Lamellaires Attribuées à*

- l'Aurignacien: Chaînes Opératoires et Perspectives Techno-Culturelles*. Luxembourg, Archéologiques 1. Actes du Symposium C6.7, XIVe Congrès de l'UISPP, Université de Liège, 2–8 Septembre 2001, pp. 375–394.
- Oksanen, J., Blanchet, F.G., Friendly, M., Kindt, R., Legendre, P., McGlenn, D., Minchin, P.R., et al., 2020. *vegan: Community Ecology Package: Ordination, Diversity and Dissimilarities*. <https://cran.r-project.org/web/packages/vegan/index.html>.
- Oliveira, D., Fernanda Sánchez Goñi, M., Naughton, F., Hodell, D., Rodrigues, T., Daniau, A.-L., Eynaud, F., Trigo, R., Abrantes, F., 2014. Understanding MIS 11 by integrating land-sea-ice records from the SHACK site (IODP 1385, SW Iberian margin). *Geophysical Research Abstracts* 16, EGU2014-13192. <http://meetingorganizer.copernicus.org/EGU2014/EGU2014-13192.pdf>.
- Olley, J.M., De Deckker, P., Roberts, R.G., Fifield, L.K., Yoshida, H., Hancock, G., 2004. Optical dating of deep-sea sediments using single grains of quartz: a comparison with radiocarbon. *Sedimentary Geology* 169, 175–189.
- Onorati, G., 1986. Découverte en Provence orientale (grotte Rainaude) d'une industrie souche de l'Aurignacien: Cette civilisation est-elle monolithique? *Bulletin de la Société Préhistorique Française* 83, 240–256.
- Onorati, G., 2006. L'émergence de l'Homme moderne en zone nord-méditerranéenne. In: de Lumley, H., Midant-Reynes, B. (eds.), Special Issue, CLIMATS-CULTURES-SOCIÉTÉS aux Temps Préhistoriques, de l'Apparition des Hominidés Jusqu'au Néolithique. *Comptes Rendus Palevol* 5, 193–202.
- Ozenda, P., 1982. *Les Végétaux dans la Biosphère*. Doin Editeur, Paris, 431 pp.
- Pétillon, J.-M., Laroulandie, V., Costamagno, S., Langlais, M., 2016. Testing environmental determinants in the cultural evolution of hunter-gatherers: a three-year multidisciplinary project on the occupation of the western Aquitaine basin during the Middle and Upper Magdalenian (19–14 kyr cal BP). *Quaternary International* 414, 1–8.
- Philippe, A., Vibet, M.-A., 2020. Analysis of archaeological phases using the R Package ArchaeoPhases. *Journal of Statistical Software* 93, 1–25. <https://doi.org/10.18637/jss.v093.c01>
- Pingree, R.D., Cann, B.L., 1990. Structure, strength and seasonality of the slope currents in the Bay of Biscay region. *Journal of the Marine Biological Association of the United Kingdom* 70, 857–885.
- Polunin, O., Walter, M., 1985. *A Guide to the Vegetation of Britain and Europe*. Oxford University Press, New York, 320 pp.
- Prescott, J.R., Hutton, J.T., 1994. Cosmic ray contributions to dose rates for luminescence and ESR dating: large depths and long-term time variations. *Radiation Measurements* 23, 497–500.
- Prüfer, K., Racimo, F., Patterson, N., Jay, F., Sankararaman, S., Sawyer, S., Heinze, A., et al., 2014. The complete genome sequence of a Neanderthal from the Altai Mountains. *Nature* 505, 43–49.
- Prüfer, K., Posth, C., Yu, H., Stössel, A., Spyrou, M.A., Deviese, T., Mattonai, M., et al., 2021. A genome sequence from a modern human skull over 45,000 years old from Zlatý kůň in Czechia. *Nature Ecology & Evolution* 5, 820–825.
- Ramsey, C.B., 2009. Dealing with outliers and offsets in radiocarbon dating. *Radiocarbon* 51, 1023–1045.
- Rasmussen, S.O., Bigler, M., Blockley, S.P., Blunier, T., Buchardt, S.L., Clausen, H.B., Cvijanovic, I., et al., 2014. A stratigraphic framework for abrupt climatic changes during the Last Glacial period based on three synchronized Greenland ice-core records: refining and extending the INTIMATE event stratigraphy. In: Rasmussen, S.O., Brauer, A., Moreno, A., Roche, D. (Eds.), Special Issue, Dating, Synthesis, and Interpretation of Palaeoclimatic Records and Model-data Integration: Advances of the INTIMATE project (INTEgration of Ice core, Marine and TERrestrial records, COST Action ES0907). *Quaternary Science Reviews* 106, 14–28.
- Rees-Jones, J., 1995. Optical Dating of Young Sediments Using Fine-Grain Quartz. *Ancient TL* 13, 9–14.
- Reimer, P.J., Austin, W.E.N., Bard, E., Bayliss, A., Blackwell, P.G., Ramsey, C.B., Butzin, M., et al., 2020. The IntCal20 Northern Hemisphere Radiocarbon Age Calibration Curve (0–55 cal kBP). *Radiocarbon* 62, 725–757.
- Reimer, P.J., Bard, E., Bayliss, A., Beck, J.W., Blackwell, P.G., Ramsey, C.B., Buck, C.E., et al., 2013. IntCal13 and Marine13 Radiocarbon Age Calibration Curves 0–50,000 Years cal BP. *Radiocarbon* 55, 1869–1887.
- Reimer, P.J., Reimer, R.W., 2001. 14CHRONO Marine20 Reservoir Database 2001. A marine reservoir correction database and on-line interface. *Radiocarbon* 43, 461–3 [WWW Document]. URL <http://calib.org/marine/> (accessed 2.25.22).
- Richerson, P.J., Bettinger, R.L., Boyd, R., 2005. Evolution on a restless planet: Were environmental variability and environmental change major drivers of human evolution. In: Wuketits, F.M., Ayala, F.J. (Eds.), *Handbook of Evolution: The Evolution of Living Systems (Including Hominids)*. Wiley-VCH Verlag GmbH & Co. KGaA, Weinheim, pp. 223–242.
- Roche, D., Paillard, D., Cortijo, E., 2004. Constraints on the duration and freshwater release of Heinrich event 4 through isotope modelling. *Nature* 432, 379–382.
- Roucoux, K.H., de Abreu, L., Shackleton, N.J., Tzedakis, P.C., 2005. The response of NW Iberian vegetation to North Atlantic climate oscillations during the last 65kyr. In: Maddy, D., Long, A.J., Bridgland, D. (Eds.), Special Issue, Quaternary Land-ocean Correlation, *Quaternary Science Reviews* 24, 1637–1653.
- Ruebens, K., McPherron, S.J.P., Hublin, J.-J., 2015. On the local Mousterian origin of the Châtelperronian: integrating typo-technological, chronostratigraphic and contextual data. *Journal of Human Evolution* 86, 55–91.
- Sánchez Goñi, M.F., Harrison, S.P., 2010. Millennial-scale climate variability and vegetation changes during the Last Glacial: concepts and terminology. In: Sánchez Goñi, M.F., Harrison, S.P. (Eds.), Special Issue, Vegetation Response to Millennial-scale Variability during the Last Glacial. *Quaternary Science Reviews* 29, 2823–2827.
- Sánchez Goñi, M.F., Eynaud, F., Turon, J.L., Shackleton, N.J., 1999. High resolution palynological record off the Iberian margin: direct land-sea correlation for the Last Interglacial complex. *Earth and Planetary Science Letters* 171, 123–137.
- Sánchez Goñi, M.F., Turon, J.-L., Eynaud, F., Gendreau, S., 2000. European climatic response to millennial-scale changes in the atmosphere-ocean system during the Last Glacial Period. *Quaternary Research* 54, 394–403.
- Sánchez Goñi, M.F., Landais, A., Fletcher, W.J., Naughton, F., Desprat, S., 2008. Contrasting impacts of Dansgaard-Oeschger events over a western European latitudinal transect modulated by orbital parameters. *Quaternary Science Reviews* 27, 1136–1151.
- Sánchez Goñi, M.F., Bard, E., Landais, A., Rossignol, L., d'Errico, F., 2013. Air-sea temperature decoupling in western Europe during the last interglacial-glacial transition. *Nature Geoscience* 6, 837–841.
- Sánchez Goñi, M.F., Desprat, S., Daniau, A.-L., Bassinot, F.C., Polanco-Martínez, J.M., Harrison, S.P., Allen, J.R.M., et al., 2017. The ACER pollen and charcoal database: a global resource to document vegetation and fire response to abrupt climate changes during the last glacial period. *Earth System Science Data* 9, 679–695.
- Sankararaman, S., Patterson, N., Li, H., Pääbo, S., Reich, D., 2012. The date of interbreeding between Neandertals and modern humans. *PLoS Genetics* 8, e1002947. <https://doi.org/10.1371/journal.pgen.1002947>.
- Sepulchre, P., Ramstein, G., Kageyama, M., Vanhaeren, M., Krinner, G., Sánchez-Goñi, M.-F., d'Errico, F., 2007. H4 abrupt event and late Neanderthal presence in Iberia. *Earth and Planetary Science Letters* 258, 283–292.
- Serryn, P., 1994. *Atlas Bordas Géographique*. Bordas, Paris.
- Shao, Y., Limberg, H., Klein, K., Wegener, C., Schmidt, I., Weniger, G.-C., Hense, A., Rostami, M., 2021. Human-existence probability of the Aurignacian techno-complex under extreme climate conditions. *Quaternary Science Reviews* 263, 106995. <https://doi.org/10.1016/j.quascirev.2021.106995>.
- Slimak, L., Zanolli, C., Higham, T., Frouin, M., Schwenninger, J.-L., Arnold, L.J., Demuro, M., et al., 2022. Modern human incursion into Neanderthal territories 54,000 years ago at Mandrin, France. *Science Advances* 8, eabj9496.
- Soressi, M., Roussel, M., Rendu, W., Primault, J., Rigaud, S., Texier, P.-J., Richter, D., et al., 2010. Les Cottés (Vienne). Nouveaux travaux sur l'un des gisements de référence pour la transition Paléolithique moyen/supérieur. In: Buisson-Catil, J., Primault, J. (Eds.), *Préhistoire Entre Vienne et Charente. Hommes et Sociétés Du Paléolithique*. Mémoire de l'Association des Publications Chauvinoises 38, 221–234.

- Stockmarr, J.**, 1971. Tablets with spores used in absolute pollen analysis. *Pollen et Spores* **13**, 615–621.
- Stokes, S., Ingram, S., Aitken, M.J., Sirocko, F., Anderson, R., Leuschner, D.**, 2003. Alternative chronologies for late Quaternary (Last Interglacial–Holocene) deep sea sediments via optical dating of silt-sized quartz. *Quaternary Science Reviews* **22**, 925–941.
- Stuiver, M., Braziunas, T.F.**, 1993. Modeling atmospheric ^{14}C influences and ^{14}C ages of marine samples to 10,000 BC. *Radiocarbon* **35**, 137–189.
- Taborin, Y.**, 1993. Shells of the French Aurignacian and Perigordian. In: Knecht, H., Pike-Tay, A., White, R. (Eds.), *Before Lascaux: the Complete Record of the Early Upper Paleolithic*. CRC Press, Boca Raton, Florida, pp. 211–227.
- Talamo, S., Aldeias, V., Goldberg, P., Chiotti, L., Dibble, H.L., Guérin, G., Hublin, J.-J., et al.**, 2020. The new ^{14}C chronology for the Palaeolithic site of La Ferrassie, France: the disappearance of Neanderthals and the arrival of *Homo sapiens* in France. *Journal of Quaternary Science* **35**, 961–973.
- Tartar, E., Teyssandier, N., Bon, François, Liolios, D.**, 2005. Equipement de chasse, équipement domestique: une distinction efficace? Réflexion sur la notion d'investissement technique dans les industries aurignaciennes. In: Astruc, L., Bon, F., Léa, V., Phillibert, P.-Y.M. et S. (Eds.), *Normes Techniques et Pratiques Sociales: De La Simplicité Des Outillages Pré- et Protohistoriques*. Antibes, France, pp. 107–117.
- Thiel, C., Buylaert, J.-P., Murray, A., Terhorst, B., Hofer, I., Tsukamoto, S., Frechen, M.**, 2011a. Luminescence dating of the Stratzing loess profile (Austria)—testing the potential of an elevated temperature post-IR IRSL protocol. In: Frechen, M. (Ed.), Special Issue, Loess in Eurasia. *Quaternary International* **234**, 23–31.
- Thiel, C., Buylaert, J.-P., Murray, A., Tsukamoto, S.**, 2011b. On the applicability of post-IR IRSL dating to Japanese loess. *Geochronometria* **38**, 369–378.
- Thomsen, K.J., Murray, A.S., Jain, M., Bøtter-Jensen, L.**, 2008. Laboratory fading rates of various luminescence signals from feldspar-rich sediment extracts. *Radiation Measurements* **43**, 1474–1486.
- Timmermann, A.**, 2020. Quantifying the potential causes of Neanderthal extinction: abrupt climate change versus competition and interbreeding. *Quaternary Science Reviews* **238**, 106331. <https://doi.org/10.1016/j.quascirev.2020.106331>.
- Tisnérat-Laborde, N., Paterne, M., Métivier, B., Arnold, M., Yiou, P., Blamart, D., Raynaud, S.**, 2010. Variability of the northeast Atlantic sea surface $\Delta 14\text{C}$ and marine reservoir age and the North Atlantic Oscillation (NAO). In: Van de Fliedert, T., Frank, M. (Eds.), Special Theme: Case Studies of Neodymium Isotopes in Paleoceanography. *Quaternary Science Reviews* **29**, 2633–2646.
- Turon, J.-L., Bourillet, J.-F., Delpeint, A., Simplet, L.**, 2004. MD141—ALIÉNOR. Rapport scientifique à bord du Marion Dufresne II. <https://www.documentation.eauetbiodiversite.fr/notice/0000000015df4b6ddfeb7c3f6ea69a3>.
- Vernot, B., Akey, J.M.**, 2015. Complex History of Admixture between Modern Humans and Neandertals. *The American Journal of Human Genetics* **96**, 448–453.
- Vielleveigne, E., Bourguignon, L., Ortega, I., Guibert, P.**, 2008. Analyse croisée des données chronologiques et des industries lithiques dans le grand sud-ouest de la France (OIS 10 à 3). *Paleo* **20**. <https://doi.org/10.4000/paleo.1715>.
- Vignoles, A., Banks, W.E., Klaric, L., Kageyama, M., Cobos, M., Romero-Alvarez, D.**, 2020. Investigating relationships between technological variability and ecology in the Middle Gravettian (ca. 32–28 ky cal. BP) in France. *OSF Preprints. Peer Community in Archaeology*. <https://doi.org/10.31219/osf.io/ud3hj>.
- Villanea, F.A., Schraiber, J.G.**, 2019. Multiple episodes of interbreeding between Neanderthal and modern humans. *Nature Ecology & Evolution* **3**, 39–44.
- Visbeck, M.H., Hurrell, J.W., Polvani, L., Cullen, H.M.**, 2001. The North Atlantic Oscillation: past, present, and future. *Proceedings of the National Academy of Sciences* **98**. <https://doi.org/10.1073/pnas.231391598>.
- Waelbroeck, C., Lougheed, B.C., Riveiros, N.V., Missiaen, L., Pedro, J., Dokken, T., Hajdas, I., et al.**, 2019. Consistently dated Atlantic sediment cores over the last 40 thousand years. *Scientific Data* **6**, 165. <https://doi.org/10.1038/s41597-019-0173-8>.
- Weber, O., Jouanneau, J.-M., Ruch, P., Mirmand, M.**, 1991. Grain-size relationship between suspended matter originating in the Gironde estuary and shelf mud-patch deposits. *Marine Geology* **96**, 159–165.
- Wintle, A.G., Huntley, D.J.**, 1979. Thermoluminescence dating of a deep-sea sediment core. *Nature* **279**, 710–712.
- Wintle, A.G., Huntley, D.J.**, 1980. Thermoluminescence dating of ocean sediments. *Canadian Journal of Earth Sciences* **17**, 348–360.
- Wolff, E.W., Chappellaz, J., Blunier, T., Rasmussen, S.O., Svensson, A.**, 2010. Millennial-scale variability during the last glacial: The ice core record. In: Sanchez Goñi, M.F., Harrison, S.P. (Eds.), Special Issue, Vegetation Response to Millennial-scale Variability during the Last Glacial. *Quaternary Science Reviews* **29**, 2828–2838.
- Wood, R.E., Arrizabalaga, A., Camps, M., Fallon, S., Iriarte-Chiapusso, M.-J., Jones, R., Maroto, J., de la Rasilla, et al.**, 2014. The chronology of the earliest Upper Palaeolithic in northern Iberia: New insights from L'Arbreda, Labeko Koba and La Viña. *Journal of Human Evolution* **69**, 91–109.
- Ziemen, F.A., Kapsch, M.-L., Klockmann, M., Mikolajewicz, U.**, 2019. Heinrich events show two-stage climate response in transient glacial simulations. *Climate of the Past* **15**, 153–168.